

FINAL PUBLISHABLE JRP REPORT

| | | |
|--|---|--|
| JRP-Contract number | New05 | |
| JRP short name | MechProNO | |
| JRP full title | Traceable measurement of mechanical properties of nano-objects | |
| Version numbers of latest contracted Annex Ia and Annex Ib against which the assessment will be made | Annex Ia: | V1.0 |
| | Annex Ib: | V1.0 |
| Period covered (dates) | From 01 September 2012 | To 31 August 2015 |
| JRP-Coordinator | Uwe Brand, PTB | |
| Tel: | +49 531 592 5111 | |
| Email: | uwe.brand@ptb.de | |
| JRP website address | http://www.ptb.de/emrp/mechprono.html | |
| Other JRP-Partners | BAM, Germany | |
| | CMI, Czech Republic | |
| | NPL, United Kingdom | |
| | VTT, Finland | |
| REG1-Researcher (associated Home Organisation) | Petra Fiala TUD, Germany | Start date:01 Sept 2012 Duration: 24 months |
| REG2-Researcher (associated Home Organisation) | Bernhard Reischl UH, Finland | Start date:01 Jun 2013 Duration: 15 months |
| REG3-Researcher (associated Home Organisation) | Karla Hiller TUCh, Germany | Start date:01 Jan 2014 Duration: 12 months |

Report Status: PU Public

TABLE OF CONTENTS

| | | |
|-----|---|----|
| 1 | Executive Summary | 3 |
| 2 | Project context, rationale and objectives | 4 |
| 2.1 | Project context and background | 4 |
| 2.2 | Objectives | 5 |
| 3 | Research results | 8 |
| 3.1 | Development of traceable stiffness calibration of AFM cantilevers in the force range of 10 pN to 1 μ N | 8 |
| 3.2 | Provision of a method for easy-to-use in-situ calibration of AFM cantilever stiffness and for instrumented indenters | 9 |
| 3.3 | Provision of three test structures with arrays of structures for a qualification of instrumented indentation technique (IIT) and AFM | 12 |
| 3.4 | Provision of Finite Element and Molecular Dynamic simulation tools to model the deformations of nano-objects from molecular level to object sizes of 100 nm to support experimental data | 15 |
| 3.5 | Performing an interlaboratory comparison on a set of test samples to reveal their mechanical properties as a first step into the creation of new types of reference materials | 17 |
| 3.6 | Provision of a guideline for the measurement of the geometrical parameters, e.g. length, diameter, width and height of nanostructures and nano-objects and to establish correction factors considering tip-sample effects | 20 |
| 3.7 | Provision of a guideline for the preparation of fixed nano-objects on hard substrates, like nanoparticles, and nanowires | 21 |
| 3.8 | Provision of a guide line for the measurement of the mechanical properties of small nanosized objects by AFM and IIT | 26 |
| 3.9 | Provision of uncertainty budgets related to the measurement of mechanical properties, such as elastic modulus | 29 |
| 4 | Actual and potential impact | 32 |
| 5 | Website address and contact details | 34 |
| 6 | List of publications | 34 |

1 Executive Summary

Introduction

The mechanical properties of nano-objects are increasingly attractive for industry, since nano-objects can be used to improve the properties of everyday materials. Several methods of mechanical measurement using atomic force microscopes (AFMs) have been developed but suffer from not being verified and traceable to the SI units. This project improved the force measurement of AFMs by developing the instrument's cantilever stiffness calibration, reducing the uncertainty of AFM elastic modulus (Young's modulus) measurements from several hundred per cent to only 30%. It also developed a new technique for the mechanical property measurement of nano-objects inside a DualBeam Focused Ion Beam (FIB)/Scanning Electron Microscopy (SEM)-device with a cantilever type force probe and provided validated reference methods that will help to develop new materials with improved mechanical strength.

The Problem

Nano-objects are used in industry to improve the mechanical properties and functionality of advanced materials, for instance to reduce weight and increase stiffness in aerospace or automotive applications or for biological applications. In the longer-term as costs come down they have the potential to be used in everyday products like glass, steel, cement, coatings and easy-to-clean ceramics. Whether the nanostructure is a layer or particles of a specific shape (nanowire, nanotube or nanoparticle) embedded in the material, it is important to know the mechanical properties and be able to measure them reliably.

Several measurement methods using AFMs have been developed to assess mechanical properties but they have not been verified and are not traceable to the SI units and therefore there is no guarantee that measurements made by different instruments, or at different times or places are comparable.

Nanoscale measurements are particularly difficult to make accurately, so by supporting experimental results with modelling and simulation the behaviour of the material can be understood and optimised. Macroscopic Finite Element Modelling (FEM) is used for macroscopic simulations and Molecular Dynamic Calculation (MDC) for the nanoscopic simulations. By extending the former towards smaller dimensions (1 μm) and the latter towards larger dimensions (100 nm) it is possible to compare the results. Instrumented indentation technique (IIT) is widely used and understood, but is not able to measure objects smaller than 500 nm. However comparative measurements between IIT and AFMs on the developed test samples, along with the modelling techniques, mean that measurement uncertainties at the nano-scale for indentation and bending can be quantified.

The Solution

The overall objective of the project was to develop measurement traceability for the mechanical properties of nano-objects such as nanoparticles, nanowires, nanoscale structures and composite materials through the development of test samples and techniques, as well as improved instruments. It focused on the key measurement tools used by the developers of nano-objects and advanced materials – AFMs and IITs.

The project developed preparation methods to fix nano-objects to substrates in order to make mechanical measurements, and developed well-defined test samples and measurement methods to verify the instruments. It developed new methods for external and in-situ force calibration, for traceable measurement of the mechanical properties of nano-objects. For AFM indentation measurements where the AFM tip radius and the contact area of the tip are needed, a blind tip reconstruction method was developed. To explore the influence of different humidity levels on nanomechanical AFM measurements, a traceable AFM with an adjustable level of humidity was developed. Additionally, the project compared measurement results from different NMIs, as the first step of establishing reference samples.

Impact

Impact was generated by

- cantilevers which are now commercially available from stakeholder NanoWorld with a stiffness uncertainty of only 10 % [1]. Using these calibrated cantilevers, force measurement uncertainty can be reduced from 20 % using the commonly used thermal vibration method. AFM users can also calibrate their own thermal vibration method on their instrument by using a reference cantilever with known stiffness.
- BAM offering a new service for the calibration of elastic modulus via Focussed Ion Beam (FIB) in-situ bending measurements of nano-beams [2].

- a new calibration service for cantilever stiffness based on calibrated MEMS [3] offered by PTB. The new calibration device is based on calibrated MEMS reference spring actuators [4] which are fabricated by Tu-Ch. Cantilevers with stiffnesses ranging from 0.01 N/m to 1000 N/m can be calibrated with an uncertainty of 5 %.
- new meander type reference springs with a very big loading area (1 mm x 0.7 mm) for force application and nearly no stiffness variation (< 1 %) when moving the loading point on this area were developed and are now commercially available for the improved in-situ AFM and nanoindenter force calibration [5].
- the development of a new MEMS double spring for AFM offering the possibility to separately calibrate force and deflection of the AFM [6]. TUCh is aiming at offering these MEMS double springs to customers in the near future.

Traceable calibrated AFM cantilevers and reduced uncertainty in stiffness will, in the long term, lead to further investigations of mechanical properties of nano-objects using AFM and help to build confidence in AFM mechanical property measurements and performance. Reliable data, combined with modelling, will allow nanomaterials to be exploited in new applications and to replace existing components. Nanomaterials have the potential to be used in the development of new materials with better mechanical properties and new functionalities; this will be facilitated by easier and more accurate mechanical property measurements. The techniques developed during the project are already being used in universities and some companies.

2 Project context, rationale and objectives

2.1 Project context and background

Nano-objects are often so small (size < 100 nm) that the well-known mechanical property measurement techniques used for macro and microscale objects, like the successful instrumented indentation technique (IIT) cannot be applied. AFM is the instrument of choice: it combines the high lateral and vertical resolution to measure nano-objects, to determine geometrical parameters like diameter, length, shape, etc., and also to perform measurements of mechanical properties like adhesion, stiffness, modulus and hardness.

In the case of small or nanoscale objects the geometry of the nano-object, especially the thickness in the case of thin films, or the diameter in the case of nanorods (NR), multiwall nanotubes (MW), and single wall nanotubes (NT), needs to be known precisely, since the measured mechanical values could drastically correlate with size (O6). Due to their small size, the mechanical behaviour of nano-objects is sometimes completely different from macroscopic objects due to their much smaller volume compared to their surface. The smaller volume leads to a reduced stiffness of the nanostructures and the relatively large surface leads to large interaction forces between tip and surface. Thus during measurement of the mechanical properties, care has to be taken not to miss these effects, which might lead to measured mechanical properties which are different from bulk values. The phenomenon is known as the 'size effect', and describes a change of the elastic modulus (Young's modulus) with decreasing size of the nano-objects.

Several AFM approaches to measure the Young's modulus of nano-objects have been published in the past 10 years. The scatter and deviation of the results amounts to more than 100 % meaning that prior to this project AFM-methods were used to map elastic modulus rather than measure it. A further problem arose since no reliable methods existed to tightly fix the nano-particles during force application by the AFM tip apex (indentation) and to prevent a slide away. Furthermore the interaction forces between tip and sample due to water layers on the sample and meniscus forming between tip and sample disturb the measurement. No methods existed to minimise these influences on the measurement results. This leads to the urgent need to develop more accurate reference techniques (O8) and the need of reference materials for the validation of methods and instruments to minimise the spread of values (O5).

The mechanical properties have to be measured with appropriate and approved techniques following standardised rules (calibrated instruments and the instruments verified for that application). This includes the calibration of cantilever stiffness (O1 and O2) and tip form, the preparation of substrates and samples (O3) in an appropriate manner and their standardisation. However, the influence of boundary conditions such as humidity and hydrophilic properties needs to be investigated.

The IIT technique for the measurement of hardness and elasticity of macroscopic specimen is reliable and can serve as a reference method to compare results obtained by AFM. IIT measurements on bulk material and on nano-objects created from that bulk material are necessary to confirm reliable IIT measurement results also on nano-objects (O8).

When measuring at the nanoscale, a number of different effects are observed simultaneously and so it is necessary to support experimental results by modelling and simulation of measurements, such as bending of single sided clamped and two sided clamped Si beams or indentation of nanowires, in order to separate out individual components of the measured response. Appropriate methods are Finite Element Modelling (FEM) and Molecular Dynamic Calculations (MDC) (O4). The former needed to be extended towards smaller dimensions (1 μm) and the latter towards larger dimensions (100 nm) in order to be able to compare the results. Successful comparisons of the test samples developed (O3) are an excellent basis for the further development of certified reference standards.

2.2 Objectives

Objectives 1 and 2 developed force calibration techniques for AFM and instrumented indenters for traceable measurement of the mechanical properties of nano-objects.

Objectives 3 and 7 established preparation methods to fix nano-objects to substrates in order to make mechanical measurements, and well-defined test samples and measurement methods to verify the instruments.

Objective 4 developed modelling of the mechanical properties to support experimental results.

Objective 5 compared measurement results from different NMIs, as the first step of establishing reference samples.

Objectives 6, 8 and 9 investigated the Instrumented Indentation Technique (IIT) and AFM techniques for the measurement of mechanical properties for real nano-objects, including the effect of humidity.

O1 Development of traceable stiffness calibration of AFM cantilevers in the force range of 1 μN to 10 pN

The ex-situ stiffness calibration of AFM cantilevers is mainly undertaken by direct calibration of the cantilever stiffness using an external calibration device like the micro-force measuring device of PTB or using a calibrated nanoindenter. Problems arise if the cantilevers are very small or if certain positions on the cantilever have to be found. To improve this situation, the available methods have to be improved and further developed.

O2 Provision of a method for easy-to-use in-situ calibration of AFM cantilever stiffness and as a method for instrumented indenters

Atomic force microscopy with its fine probe combined with measurements of various physical forces, is able to measure both size and force. The force is calculated as the product of the measured deflection of the AFM cantilever and its stiffness. The cantilever stiffness can be calibrated in-situ and externally. The most often used in-situ calibration method is the thermal vibration method. Here the vibration spectrum of the cantilever is measured and from this, and the temperature of the air, the stiffness can be calculated with an uncertainty of 20 %. Publications show that in experiments usually deviations of up to 50 % are observed [7].

Another in-situ calibration technique is the cantilever on reference cantilever method where calibrated reference cantilevers are used. A problem with this technique, is that the stiffness of reference cantilevers strongly depends on the probing position on the cantilever, since their stiffness depends on the third power of the length of these beams. Thus the use of this technique is not easy and the achievable uncertainty is limited to 10 %.

Most of the available stiffness calibration techniques were developed for applications in air. Biological specimen have to be measured in liquid and thus corresponding techniques in liquid were also developed and have to be evaluated. The project aimed to develop a novel type of device which can be applied in situ to calibrate the stiffness of the cantilever with an uncertainty of less than 5 %.

O3 Provision of three test structures with arrays of structures for qualification of IIT and AFM

Nanostructured test samples with well-known properties can be very well used to verify IIT and AFMs with respect to Young's modulus. Samples where the homogeneity of the mechanical properties has been checked by IIT can be structured by Focussed Ion beam (FIB) and by E-Beam-Lithography (EBL) to create arrays of pillars and beams of different sizes. The beams can be of single sided clamped or double sided clamped type with the same thickness but different lengths and widths. The well-defined structures enable appropriate modelling to be undertaken using Finite-Element-Modelling and allow the project partners to investigate the applicability of IIT to smaller object sizes and to compare them with the AFM results.

O4 Provision of new Finite Element and Molecular Dynamic simulation tools to model the deformations of nano-objects from the molecular level up to object sizes of 100 nm to support experimental data

At the microscale the Finite Element Method (FEM) is mostly performed by using well-known material parameters from homogeneously large bulk materials. For molecular dynamics calculations (MDC) the known properties of binding energies, length and angle are used to derive interatomic potentials which are then used to calculate the forces between all the atoms involved in a constructed small nano-object. Due to the large calculation time required and to problems related to large dimensions, MDC is generally limited to small objects, otherwise very fast computers and long calculation times are required. This objective additionally investigates effects of water layers due to condensation from the air.

O5 Performance of an interlaboratory comparison on a set of test samples to determine their mechanical properties as a first step towards the creation of new types of reference materials

Currently, a great variety of new techniques exist for the calibration of the stiffness of AFM cantilevers, and also for the measurement of mechanical parameters like Young's modulus, hardness and adhesion with AFMs. These new techniques need to be tested and validated in order to be accepted world-wide. This requires international comparison measurements. These comparisons only make sense if well prepared samples can be used, if precise descriptions of the measurement methods are available, if the boundary conditions are clear and if the evaluation of the data is internationally accepted.

O6 Provision of a guideline to measure the geometrical parameters, e.g. length, diameter, width and height of nanostructures and nano-objects and to establish correction factors for tip-sample effects

The geometrical parameters, length, width, diameter and height of nano-objects are needed for various methods to determine mechanical properties. For example when applying bending tests to determine the Young's modulus of small beams the geometrical properties of the beam are needed. The length and width of beams should be easily measurable by AFM, but not their thickness. To determine the thickness of beams the idea is to make the beams from membranes or layers and to determine the membrane or layer thickness by x-ray reflectometry (XRR) or transmission electron microscopy (TEM).

Factors which might influence the measured width and height of nano-objects are AFM tip radius and shape, material of tip and sample, operation mode of the AFM (contact, tapping, non-contact mode) and the humidity level during measurement.

O7 Provision of a guideline for the preparation of nano-objects attached to hard substrates, such as nanoparticles, and nanowires

In order to reliably measure the mechanical properties of nano-objects, indentation measurements at the nano-objects have to be made. If the probed surface area is not aligned perpendicular to the acting force, then lateral forces are created, which might move the measured particle during indentation. To prevent this, different techniques to fix the objects to a substrate must be investigated.

The properties of nanoparticles fixed or embedded in a layer have to be measured by different techniques in order to evaluate the fixing methods.

O8 Provision of a guideline to measure the mechanical properties of small nanosized objects by AFM and IIT

The mechanical properties of samples near the surface can be measured by IIT and different AFM techniques. For accurate nanoindentation measurements using Vickers and Berkovich indenters, the contact area of each indenter has to be measured. Usually reference materials with known Young's modulus are used to measure the contact area. These reference materials are also used to measure the compliance of the instruments. Due to the high stiffness of nanoindenters of usually some MN/m, this

compliance is of the order of only some nm/mN. For AFM the instrument stiffness is mainly given by the stiffness of the cantilever which is of the order of only some N/m and thus much weaker than that of nanoindenters. This places a further emphasis on the high precision determination of the cantilever stiffness.

O9 Provision of uncertainty budgets for the measurement of mechanical properties, such as elastic modulus

Evaluating uncertainty budgets requires comparison measurements. The weighted average value of several measurements serves as a reference value. The difference of the measurement result to be evaluated to the reference value is compared with the stated measurement uncertainty of this technique. If the difference is higher than the uncertainty, then the stated measurement uncertainty is too small and has to be increased.

In this objective the uncertainty budgets of two different techniques to measure the elastic modulus of nano-objects were evaluated. For the indentation technique with Oliver and Pharr evaluation and the beam bending technique the achievable measurement uncertainties were estimated. Comparison measurements are supplied by the well-known IIT indentation technique.

3 Research results

3.1 Development of traceable stiffness calibration of AFM cantilevers in the force range of 10 pN to 1 μN

Objective achieved - Traceable stiffness calibration of AFM cantilevers has been achieved using an improved thermal vibration method. An AFM cantilever calibration service is now offered at NanoWorld Services GmbH with a validated uncertainty of 10%.

Forces from several pN to μN can be measured by atomic force microscopes (AFM) if the normal stiffness of the cantilever is known. Therefore a great variety of methods to calibrate this stiffness have been developed during the past two decades. The most widely used method, which is non-destructive for the cantilever apex and is implemented in nearly each commercially available AFM, is the thermal vibration method. Although the uncertainty in stiffness is estimated at 15 - 20 % and the method is standardised in ISO 11775, deviations to other methods of up to 50 % have been observed. Thus together with the collaborator NanoWorld Services GmbH, PTB improved the widely used thermal vibration method for the calibration of the bending stiffness of AFM cantilevers with stiffnesses ranging from 0.01 N/m to 5 N/m from 50 % to 10 % uncertainty. A laser vibrometer was used to measure the amplitude spectrum of the cantilever at room temperature. This spectrum is then converted into the power spectral density (PSD). The force constant, resonance frequency and quality factor are determined by fitting a simple harmonic oscillator function to the resonance peak curve in the PSD. NanoWorld uses a self-developed force standard chip, the CalibLever [1] (s. Fig. 1), to calibrate its thermal vibration method. Three rectangular cantilevers without a tip but with marks to identify the loading position on the levers are on the CalibLever. The stiffness of the “long” and the “middle” cantilevers (nominal stiffnesses: $k_{long} = 0.23$ N/m and $k_{middle} = 2.6$ N/m) were calibrated by PTB using the traceable PTB microforce measuring device. The two calibrated cantilevers then served as reference cantilevers for the calibration of the thermal vibration method. NanoWorld states an uncertainty for the improved thermal vibration method of $U(k) = 10$ % (confidence level 95 %).

In order to evaluate this improved thermal vibration technique the stiffness of three different types of rectangular AFM cantilevers (PPP-NCST-3, PPP-FM-3, PPP-CONT-3) were measured by PTB and by NanoWorld using the improved thermal vibration method. PTB used the MEMS active reference spring method ($k_{C,MEMS}$) based on a MEMS actuator with a stiffness of $k_{MEMS} = (3.24 \pm 0.13)$ N/m and on a random basis also by PTB’s microforce ($k_{C,PTB,MFMD}$) measuring device. The difference between the two PTB measurements is less than 4 %, confirming the measurement uncertainty of the new MEMS reference spring method. The mean deviation of the values measured using the improved thermal vibration method from those of the MEMS-based stiffness measurement is + 6.9 % with a standard deviation of 2.9 %.

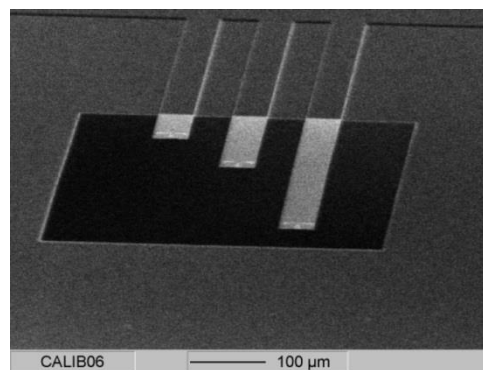


Fig. 1 Reference cantilever chip CalibLever with three rectangular cantilevers of different length and hence different stiffness (0.23 N/m, 2.6 N/m and 40 N/m)

Compared with the conventional thermal vibration method, the improved thermal vibration method shows a smaller mean deviation from the MEMS values and a reduced scattering of the values. Thus these values confirm the stated measurement uncertainty of 10 % for the improved thermal vibration method. NanoWorld now offers a service of AFM cantilever calibration with an uncertainty of normal spring stiffness of 10 %. The work on this topic was published in a contribution entitled “Comparing AFM cantilever stiffness measured using the thermal vibration and the improved thermal vibration methods with that of an SI traceable method based on MEMS” to the journal Measurement Science and Technology [7] (Brand et al., 2016).

3.2 Provision of a method for easy-to-use in-situ calibration of AFM cantilever stiffness and for instrumented indenters

Objective achieved – Methods for in-situ stiffness calibration of AFM cantilevers and for instrumented indenters have been developed, based on the cantilever on reference spring method. The reference springs are available from CiS GmbH and PTB with a force uncertainty of 4 % or even 2 %.

The precise and well-known cantilever on reference cantilever method for the calibration of AFM cantilever stiffness suffers from the fact that the stiffness of these reference cantilevers depends to the third power on the loading position. To improve this drawback, two new reference springs, one for AFM and one for instrumented indenters were developed.

For AFM a new MEMS reference spring offering the possibility to separately calibrate force and deflection was developed. The new MEMS spring consists of two springs in series with a gap of 3 μm [6]. The big advantage of these new MEMS reference springs is that they show no dependence of stiffness on the loading position on the MEMS loading area (60 μm x 50 μm) and moreover the temperature dependence of stiffness, force and deflection is below 1 % for ambient conditions. TU-Ch is aiming at offering these MEMS double springs to customers in the near future. Force uncertainties down to 2 % can be obtained using these reference springs.

For instrumented indenters a meander spring with a stiffness of 15 N/m was developed. The linearity deviations up to 1 mN force are smaller than 0.2 % and more importantly, the influence of the loading position on the stiffness is strongly reduced (< 1 %) compared to cantilever type reference springs (10 – 20 %). The reference springs will be available from CiS GmbH in near future. These springs can also be used with AFM and force uncertainties down to 4 % are possible using these springs.

MEMS double spring for simultaneous calibration of force and deflection of AFMs

An existing MEMS array was used to create a double spring. The MEMS contact area for the forces to be applied to the MEMS double spring had to be FIB polished by BAM in order to smooth its surface. The MEMS double spring consists of two springs, which are separated by approximately 3 μm (Fig. 2). The thickness of the spring elements was 4 μm and the height of the structures was 50 μm . The contact areas of both springs are of cylindrical form. Together with the high precision of lithography processing this ensures good contact conditions and should lead to small pull-off forces. The main advantage of the developed MEMS double spring should be the small dependence of the measured stiffness on the location of the force loading point on the contact area of the double spring. This is because the MEMS shaft is suspended by four symmetrically arranged folded springs (s. Fig. 2) which lead to a linear movement of the contact area.

A further advantage of the described silicon MEMS double spring is the expected low dependence of its calibration values (stiffness, bending force and bending deflection) on temperature. For a bending deflection of 3 μm and a thermal expansion coefficient of silicon of $2.3 \cdot 10^{-6} \cdot \text{K}^{-1}$, the expected thermal change of the bending deflection is only 6.9 pm/K. Under ordinary laboratory conditions this contribution will be sufficiently small and can be neglected.

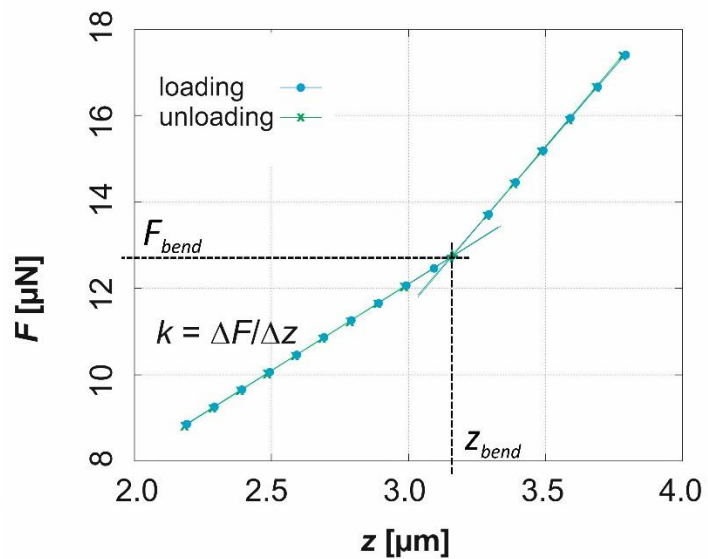
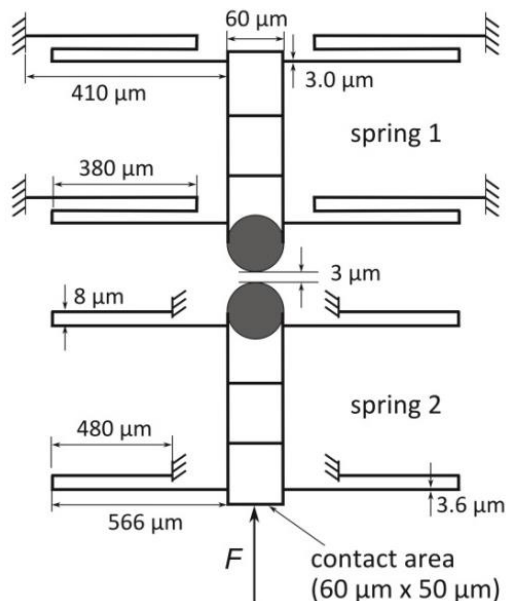


Fig. 2 MEMS shaft after FIB processing. The lower face of the shaft is the contact area of the double spring

Fig. 3 Determination of the inflexion of the loading and the unloading curve (+: inflexion point)

PTB's microforce measuring device was used to measure the force deflection curve of the double spring. It consists of a compensation balance with a measurement range of 2 g which corresponds to a maximum force of 20 mN, a nanopositioner with 100 μm maximum displacement and 1 nm resolution, a hard metal stylus with a 300 μm diameter ruby probing sphere which was mounted on the balance pan, and a holder for the MEMS spring which was fixed at the nanopositioner and can be positioned in x- and y-direction by a motorised xy-table. The temperature of the laboratory is stabilised to ± 0.1 K. During the experiment the air temperature, the relative humidity and also the air pressure inside the box are measured. The uncertainty of this device for measuring stiffness is estimated at 4 % [9]. Main contributions to this uncertainty are the deflection measurement with 3.5 % and the force uncertainty contribution with 2 %.

Force-deflection measurements were carried out in the centre of the MEMS contact area and along two perpendicular lines in x- and y-direction. A typical force deflection curve consists of the loading curve in which the deflection z is increased until maximum, and of the unloading curve in which the deflection is decreased in the same manner. Three parameters were determined for each loading and unloading force deflection curve:

- the bending stiffness k of the curve up to the inflexion point, and
- the force F_{bend} and deflection z_{bend} at that inflexion point, which we call here bending force and bending deflection.

The bending stiffness is determined by a linear regression of the curve up to the inflexion point. The inflexion point is determined by calculating the intersection of the two regression lines through the points below and above the inflexion point (Fig. 3). The bending stiffnesses of loading and unloading curves have been determined in the force range from 1 μN to 11 μN.

Thermal drifts during a measurement lead to changes in the measured bending deflection and stiffness. In order to investigate this effect, after 23 hours measuring at a temperature of 22.1°C the temperature inside the measurement chamber was increased by switching on a LED light. The temperature rose within a few hours to 22.5°C, then to 22.6°C, and finally to 22.7°C. The averaged parameters determined at these temperatures deviate by not more than 0.2%. This corresponds to a parameter change of less than 0.4%/K. This deviation is one order of magnitude smaller than the measurement uncertainties U of the parameters ($U(k) = 4\%$, $U(F_{bend}) = 2\%$ and $U(z_{bend}) = 3.5\%$). Thus a temperature change inside the measurement chamber of +0.6 °C does not lead to a measurable change in the calibration parameters of the double spring. Moreover the average nonlinearity of the spring is only $\pm 0.1\%$ in the force range up to 11 μN. The work on this topic was published in a contribution entitled "Silicon double spring for the simultaneous

calibration of probing forces and deflections in the micro range” to the journal Measurement Science and Technology ([6] Brand et al., 2016).

With these new MEMS double springs it is possible to traceably calibrate forces of AFM with an improved uncertainty of 2 %.

3.2.2 Meander reference springs for force calibration of nanoindenters

The force calibration of nanoindenters is possible in the mN-range up to 500 mN using commercially available silicon reference springs. In the μN -range there was no suitable standard available. Thus a new silicon reference spring was developed for that range in cooperation with the IHT of Braunschweig Technical University. It is based on meander spring elements in a bridge type beam standard (s. Fig. 4).



Fig. 4. Photo of the new silicon meander reference spring

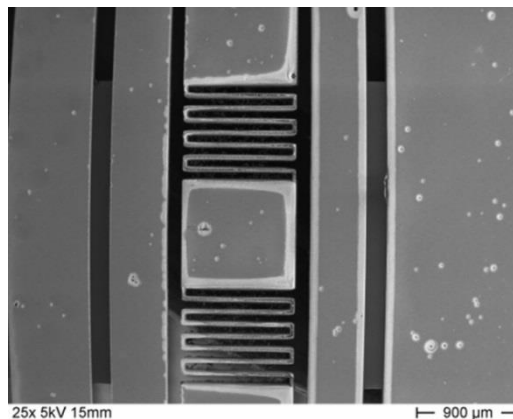


Fig. 5. SEM image of central boss and the meander springs of the new meander reference spring

The central probing area has a size of 0.7 mm x 1.0 mm (s. Fig. 5). The stiffness change when varying the loading position on the central probing area was investigated by scanning the loading position in both lateral directions, in beam direction and perpendicular to it. The measured stiffness in the center of the central probing area changes by only -0.7 % when moving the loading point by $\pm 300 \mu\text{m}$ out of the center in beam direction. The stiffness change was even smaller (-0.13 %/ $\pm 300 \mu\text{m}$) when moving the loading point perpendicular to the beam direction. The stiffness of these springs amounts to 15 N/m. The maximum force investigated was 900 μN . The measured nonlinearity of these springs amounts to 0.2 %. The work on this topic was published in a contribution to the proceedings of the SPIE conference 9517 entitled “Smart sensors and calibration standards for high precision metrology” [5] (Brand et al., 2015).

This reference spring offers also sensor functions. In the outer bending areas of the bridge piezoresistive full bridges are located. Both Wheatstone bridges supply an output voltage proportional to the deflection of the central boss. Investigations are underway to fully characterise these sensors.

A comparable meander spring design was fabricated by the CiS GmbH, a cooperation partner of PTB and will be commercially available in near future.

With these new meander type reference springs it is possible to traceably calibrate indentation forces of nanoindenters with an improved uncertainty of 4 %. This value is limited by the uncertainty of its stiffness calibration

3.3 Provision of three test structures with arrays of structures for a qualification of instrumented indentation technique (IIT) and AFM

Objective achieved - The MechProNO partners provided arrays of pillars, beams, wires and nano-particles which were used for comparisons of IIT and AFM, with no size effects observed.

Pillars

Pillars of two different materials were fabricated using silicon microtechnology, silicon and photo-resist. IIT measurements at PTB and BAM on high aspect ratio silicon pillars revealed that the equivalent stiffness of the pillars has to be taken into account in order to prevent systematic errors of the measured Young's modulus. The equivalent stiffness is proportional to the square of the pillar radius and inversely proportional to pillar height. Both, pillar diameter and height were measured using NPL's traceable dimensional AFM. Taking the equivalent pillar stiffness into account, Young's moduli comparable to the bulk material resulted. Ignoring this effect led to decreased indentation moduli down to 35 % of the bulk value. Thus, no size effect is observed. The work on this topic was published in a contribution entitled "Determination of the mechanical properties of nano-pillars using the nanoindentation technique" to the journal Nanotechnology and Precision Engineering ([10] Li et al., 2014).

Beams

Two commercially available materials, amorphous silicon oxide and amorphous silicon nitride, have been identified as suitable for future reference materials for the following reasons: the specimens provide both free standing membranes and coatings on silicon substrates. The latter can be used for IIT-measurements, whereas beams of different length and width can be cut from the former by FIB machining. BAM developed a new technique for in-situ bending in a DualBeam FIB/SEM-device. The method is based on a micromanipulator with piezoresistive cantilever force sensor for force application and measurement, as well as a digital image correlation software for the evaluation of beam displacements. Thus, at least two independent methods could be applied to the same material for Young's modulus determination. The measured Young's moduli agreed to within 20 % and no size effect was observed.

Provision of test structures by Focused Ion Beam Machining

Focused ion beam (FIB) machining is a standard technology for the preparation of thin lamellae from a large variety of bulk materials for further characterisation by Transmission Electron Microscopy (TEM). The idea was to use this technique not only for microstructural characterisation, but also for the preparation of well-defined nano-objects which then will be available for further measurements of mechanical properties by IIT- or AFM-based methods.

Standard TEM-lamellae are already nano-objects. Although the lateral dimensions of such beams are in the range of several microns, their thickness can be well below 100 nm. The problem with standard TEM-lamellae is that their thickness is not well defined and usually not uniform over the whole object. However, the thickness is one of the critical geometry parameters, which should be known as exactly as possible. Therefore, we had to search for a solution for obtaining beams with uniform thickness. The idea was to use membranes produced by coating of a silicon wafer with either amorphous silica or silicon nitride and subsequent etching of a window through the thin silicon wafer, thus producing an area of 100 x 100 μm^2 of a free standing membrane. Such specimens of silicon oxide and silicon nitride membranes are commercially available in different thicknesses. We used such specimens as starting point for preparing nanobeams for AFM-measurements. Later we could show that the same specimens can be used for IIT and a new type of testing method inside the FIB consisting of a Kleindiek force sensor (see objective 5).

Beams of different lengths, widths and thicknesses were prepared within a theoretical stiffness range (assuming bulk properties of the respective materials) suitable for AFM measurements. Unfortunately, most of the thin SiO₂ beams were twisted after having been cut from the membrane due to internal stress within the membrane and therefore could not be used for further measurements. The silicon nitride beams were not twisted, at least down to a thickness of 100 nm, and therefore were used for measurements (see objective 5).

A problem with all FIB-prepared test structures was that, since manually machined, they all represent single individual objects which were difficult to handle and to measure accurately with both IIT and AFM methods.

The as-prepared objects were bent with a Force-Measurement-System (FMS) from Kleindiek Nanotechnik, Germany. This system is an extension tool for a micromanipulator from the mentioned supplier (Fig. 6a). The tool is equipped with a 400 μm long silicon cantilever, containing piezo-resistive sensors for deflection measurement. Deflecting the cantilever a signal depending on the actual contact force is generated by the sensor. The FMS is mounted in the vacuum chamber of the DualBeam machine. Every process step can be observed by SEM.

Before starting to measure on the object, the system has to be calibrated. Therefore a certified calibration spring from PTB with known spring constant (k_1) is displaced exactly 1 μm (Fig. 6b left). Together with the detected voltage a calibration value is calculated. All measured voltages are then multiplied by this calibration value and give the corresponding force value. To check whether this calibration value is plausible a second calibration spring with known spring constant k_2 (Fig. 6b right) is also displaced 1 μm . Then forces between 8 μN and 9.8 μN are measured, which indicates a relatively high standard deviation for the force measurement of about 10 % but no systematic deviation of the average force was measured.

A second parameter had to be checked before starting measurements, the stiffness of the used cantilever. During the test, bending of the cantilever should not take place. Therefore a maximum loading force for the FMS was determined experimentally. A calibrated microelectromechanical system (MEMS) device from PTB with a moveable main shaft was displaced about 6 μm (Fig. 6c). The stiffness of the MEMS is stable until a maximum displacement of 8 μm . When comparing both the theoretical and the measured force-displacement curves it becomes obvious that the slope (stiffness) is equal until a maximum force of about 7 μN . With higher forces the slopes differ more and more, which indicates that the cantilever of the FMS is bent.

The objects can then be tested (Fig. 6d). Unfortunately the system offers no automatic solution to apply constant forces or loading rates. Thus the objects could be bent manually via driving knobs moving the micromanipulator in the three axes. However, preliminary tests showed that the manual bending with different bending speeds did not influence the resulting value significantly. The measured forces had to be correlated with the corresponding displacements. The displacements were measured with the image correlation software VEDDAC from Chemnitzer Werkstoffmechanik GmbH applied to a series of images taken every second during the bending test by the SEM.

The new method was tested and compared with IIT by using the silicon nitride beams described above. The results are reported under objective 5.

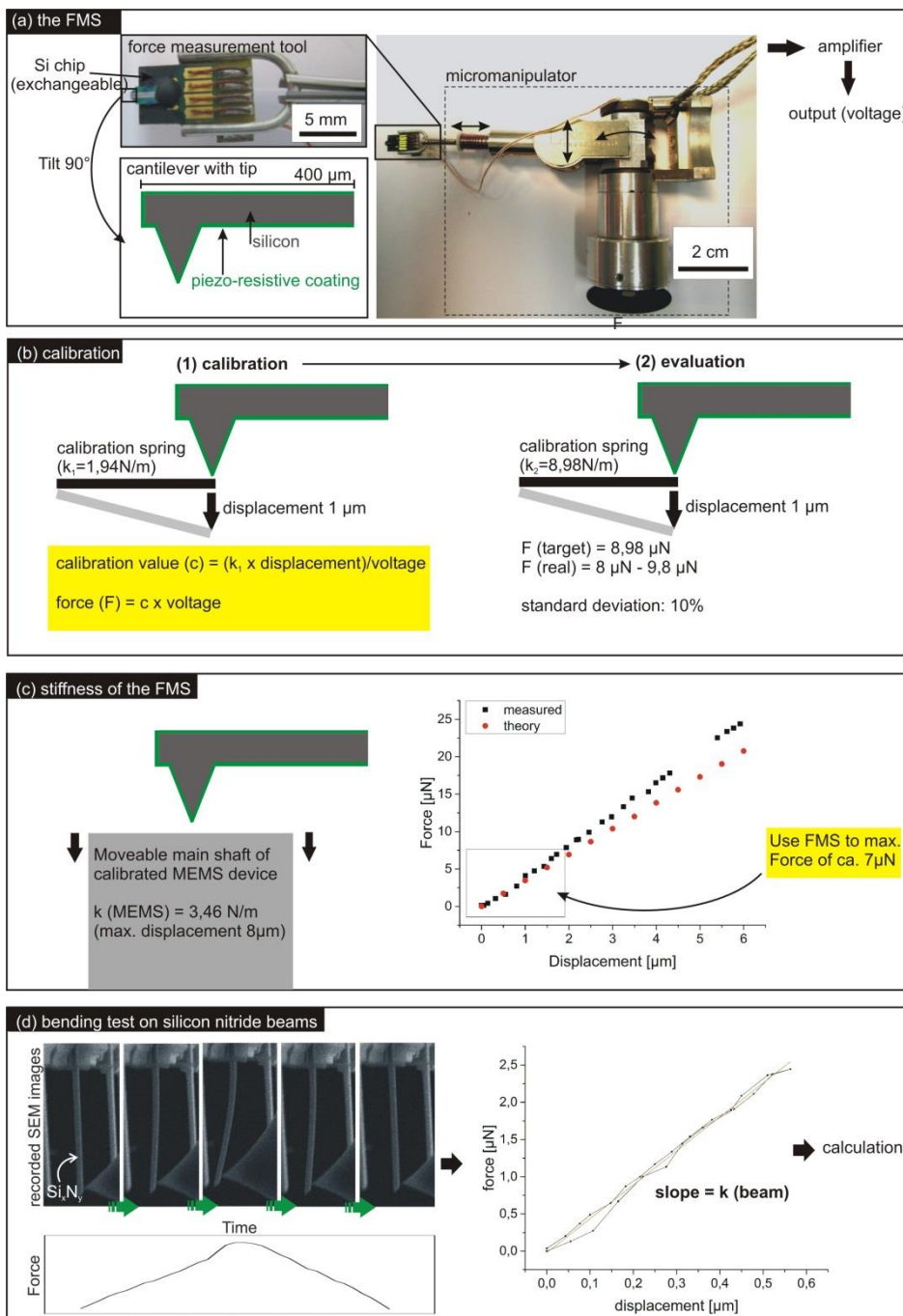


Fig. 6 (a) BAM's FMS force measurement setup inside a FIB and the measuring principle; (b) calibration procedure; (c) checking the stiffness of the system with a calibrated MEMS; (d) silicon nitride beam bending experiment

Silicon nanowires

Furthermore, the method was applied to silicon nanowires which were supplied by Prof. Alaca from Koc University, Istanbul. Since these nanowires were made by an etching technique from a well-known material (Si wafer) in a well- defined orientation <110> they were suitable for a validation of our in-situ testing method. It was shown that it is possible to prepare double-anchored silicon nanowires, where nanowires and their supports were etched from the same silicon crystal. This eliminated any interface compliance, which would hinder the accuracy of nanomechanical characterisation results. Nanowire cross-sections had trapezoidal or pentagonal shapes. The maximum nanowire width utilised in this study was 74 nm, whereas

a minimum of 35 nm could be achieved. Three-point bending tests were conducted on the nanowires within the FIB/SEM chamber via a force sensor probe. The measured force-displacement curves yielded good correlation in comparison to simulated force-displacement curves with the modulus of elasticity taken as the bulk $\langle 110 \rangle$ value of 169 GPa. Small deviations between successive tests can be explained by uncertainties of tip positioning and, specifically in the case of smaller nanowires, twisting of the nanowire. A further slight systematic deviation observed for the smallest wire was attributed to the influence of the very small native oxide layer. In conclusion no size effect of the elastic behavior of silicon was found in this study. The work on this topic was published in a contribution entitled “Determination of the Elastic Behavior of Silicon Nanowires within a Scanning Electron Microscope” to the journal *Nanomaterials* ([2] Wollschläger et al., 2016).

3.4 Provision of Finite Element and Molecular Dynamic simulation tools to model the deformations of nano-objects from molecular level to object sizes of 100 nm to support experimental data

Objective achieved – Atomistic model systems of gold nanorods have been built and used to simulate AFM nanoindentation experiments, showing how dislocations nucleate, move and annihilate or are trapped in the nanorods and how the crystal orientation affects the deformation mechanism.

Atomistic model systems of gold nanorods and a diamond AFM tip with 5 nm radius have been built and molecular dynamics (MD) simulations of AFM nanoindentation experiments were carried out. Force-distance curves were simulated showing how dislocations nucleate, move and annihilate or are trapped in the nanorods and how the crystal orientation affects the deformation mechanism.

When determining the mechanical properties of a thin film the penetration depth must be as small as possible so that the deformation zone does not exceed the thickness of the film. For small depths, the results may be significantly distorted by the roughness of the thin film. The effects of roughness on the reduced modulus were investigated using 3D FEA modeling to map the apparent modulus on a real rough surface as measured by AFM.

MD simulations of gold nanorods

Atomistic molecular dynamics was used to simulate the indentation of gold nanorods of different crystallographic structure with a diamond AFM tip. The simulations indicate that both, the structure and the orientation of the sample affect the atomistic mechanism of the indentation. The initial mechanism of dislocation nucleation under the area of indentation is similar to the indentation of a bulk surface. However, after indentation depths as small as a nanometer, the force–distance curves observed on the nanorods increase less steeply as on the corresponding bulk surfaces (s. Fig. 7), as dislocations can glide easily towards the sides of the nanorods, leading to plastic deformation and stress release. The details of these atomic scale processes depend on nanoscale fluctuations, as well as finite-size effects.

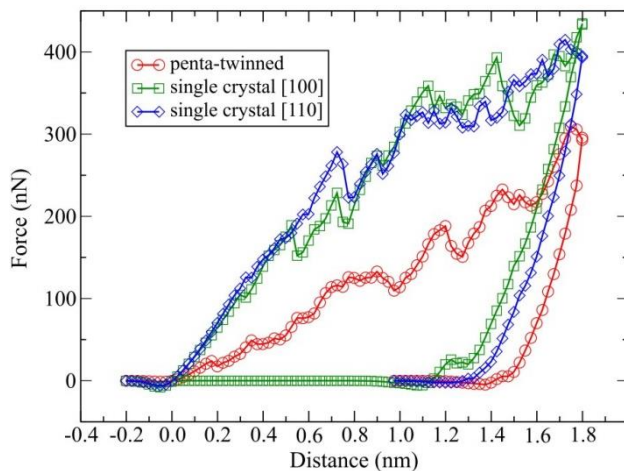


Fig. 7 Force–distances curves for the loading and unloading cycle obtained with a frozen tip on single crystal and penta-twinned gold nanorods, with diamond AFM tips of 5 nm radius

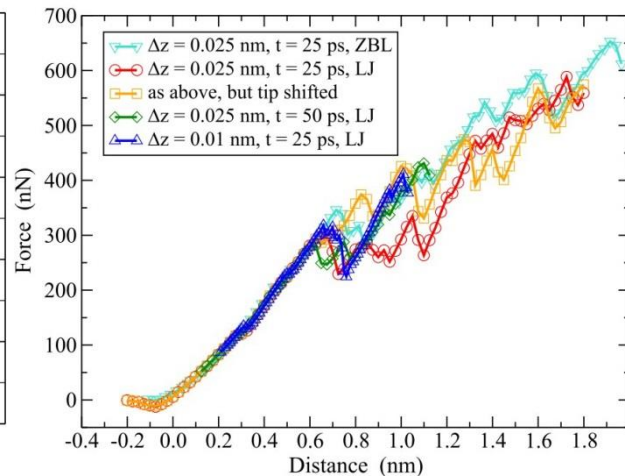


Fig. 8 Influence of simulation parameters on the force–distance curve when indenting a single crystal gold nanorod exposing the (100) facet (tip radius $r = 5$ nm). The type of Au–C interactions (Lennard-Jones or ZBL), indentation depth increment (Δz), MD trajectory length (t), and lateral position of the AFM tip all influence the force–distance curve beyond the initial elastic regime, but not significantly.

It was found that the AFM tip apex radius of curvature strongly affects the forces on the single crystalline nanorods exposing flat facets, but is less important when indenting penta-twinned nanorods exposing only an edge to the tip. Furthermore the deformation mechanism depends only on the nanorod structure and orientation, not on the tip radius.

In terms of implications for experiments, determining the orientation of a sample from the force – distance curve may not be possible, as the curves can exhibit a very similar profile, such as for the (100) and (110) facets of the single crystal nanorod, even though the deformation mechanism is very different. However, the shape change of the nanorod under load may be visible in subsequent high resolution AFM imaging of the sample in amplitude or frequency modulation mode, using the same tip. The work on this topic was published in a contribution entitled “Nanoindentation of gold nanorods with an atomic force microscope”, Mater. Res. Express” to the journal Materials Research Express ([11] Reischl et al., 2014).

Modelling the influence of roughness on nanoindentation data using FEM

With nanoindentation ISO 14577-4 recommends that the roughness, R_a , should be less than 5 % of the maximum indentation depth. However, in many cases this may not be feasible. Especially for soft samples or thin films where a low load is needed, this approach may not be useful. The interplay of roughness and mechanical properties is very tricky for elastic modulus maps. Because the morphology affects the measured modulus value, special care must be taken to separate these effects. This is a common problem with scanning methods. From a metrological point of view, this unknown influence of roughness acts as a source of uncertainty. The exact topology of the surface of the indented sample is unknown, which affects both the measured result and its uncertainty.

The work showed a direct effect of the morphology on the apparent modulus. The elastic modulus can be seen to be smaller in a concave area of the profile and larger in a convex area. The qualitative trend is similar, with three major aspects. Firstly, the FEA calculation shows more noise, which is to be expected since it uses the raw, unsmoothed morphology as its input. Secondly, the minima of the Hertzian model are lower than those of the FEA model, probably due to a combination of the facts that the smoothing process

somewhat flattens the surface and the reduced modulus has been normalised. Thirdly, there are spikes on the reduced modulus curve for which the curve of the Hertzian model has no counterparts. These spikes occur at approx. the inflection points of the height curve and correspond to approx. half of the height of the asperity, thereby illuminating one of the limitations of the Hertzian model — especially its use of the mean curvature — in that it does not correctly distinguish between extrema and saddle points. The variances found by the Hertzian model and the FEA model differ by only a few percent and are lower by approx. 30 % than the variance found by experiment [12].

3.4.3 Application of FEM to support experimental data of silicon wire bending

Part of the work on silicon nanowires (s. 3.3) was verification of test results by FEM modelling. This task was done by Zuhail Tasdemir from Koc University within a cooperative research on silicon nanowires. The fabrication of the nanowires is published in a contribution entitled “A deep etching mechanism for trench-bridging silicon nanowires” to the journal *Nanotechnology* ([13] Tasdemir et al., 2016). The nanomechanical characterisation of the wires and the comparison with FEM was published in a contribution entitled “Determination of the Elastic Behavior of Silicon Nanowires within a Scanning Electron Microscope” to the journal *Nanomaterials* ([2] Wollschläger et al., 2014). Firstly, it was clearly shown that it is most important to consider the complicated shape of the nanowires. The assumption of a simplified rectangular cross-section led to a major deviation from the experimental data obtained by in-situ bending tests. Secondly, a slope change of the experimental force-displacement-curve at displacements greater than 100 nm was observed for the smallest nanowires. From the SEM results it seemed that twisting of the nanowire has taken place due to difficulties in positioning the cantilever tip on the very small area of the testing object. The twisting and corresponding slope change could be simulated with FEM by changing the site of the applied force from the top to the side wall. Thirdly, a slight impact of the 4 nm thick native oxide layer on the force-displacement-curve of the small wire was also simulated.

3.5 Performing an interlaboratory comparison on a set of test samples to reveal their mechanical properties as a first step into the creation of new types of reference materials

Objective achieved – An interlaboratory comparison of Young’s modulus was performed with FIB fabricated silicon nitride beams, confirming the comparison of two bending methods and nanoindentation within 20%. Thus silicon nitride beams are an ideal candidate for new reference materials.

An interlaboratory comparison was performed with FIB fabricated silicon nitride beams made of membranes. The thickness was measured with an uncertainty of 3 % by TEM at BAM. BAM used the in-situ FIB bending test and IIT and PTB the MEMS-based bending method. The Young’s modulus of the two bending methods agree to within 6 % and the Young’s modulus measured by IIT is 20 % higher [26].

Interlaboratory comparison of FIB fabricated silicon nitride beams

During the project PTB developed a MEMS-based force measurement technique. It includes calibrated MEMS with moveable main shaft. At the very end of the main shaft (area 50 μm x 50 μm) a sphere with known radius was glued to generate a single contact point during the following bending test. BAM provides a 515 nm thick silicon nitride beam with 2 μm width and 15 μm length prepared by FIB machining. This beam was bent in the SEM with the cantilever-based FMS as described above. The mean Young’s Modulus calculated from these tests was (185 \pm 15) GPa. Afterwards PTB tested the same beam with their system and calculated a value of (174 \pm 17) GPa. Both results are in good agreement concerning the sources of error and uncertainties. Fig. 9 shows in overview the MEMS-based system.

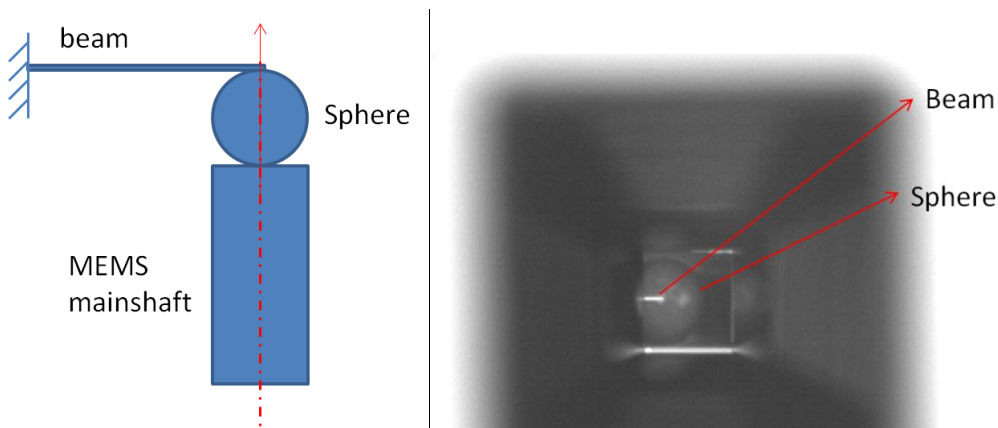


Fig. 9 Left: schematic of the testing set-up of the MEMS-based system; right: light-microscopic image during the testing; the light rectangle represents the silicon nitride beam in the etched silicon square. The round object is the sphere glued to the main shaft. Positioning was done by moving the MEMS.

FIB fabrication of silicon nitride beams

The silicon nitride membranes with nominal thicknesses of 50, 100, 200 and 500 nm were used for a comparison of Young's Modulus determination with two independent methods, the in-situ bending method, and IIT. This is not an interlaboratory comparison, but it serves the same objective, to do a first step into the creation of a new type of reference materials. The silicone-nitride samples were selected because untwisted beams could be produced at least in the thickness range from 50 nm to 500 nm, as shown in Fig. 10a.

Fig. 10 shows thicknesses and interfacial situation with the silicon substrate for the different silicon nitride films and the results of bending tests determined by inserting the experimentally determined geometrical parameters of the cut-out beams, the forces and corresponding displacements into the Euler-Bernoulli equation.

It has to be pointed out here that beam thicknesses and interfacial situation can deviate significantly from nominal values, and thus have to be checked thoroughly before evaluation of experimental results. This is especially the case for the nominally 200 nm thick film. Here the real thickness measured by TEM was 182 nm and a 250 nm thick SiO₂ interlayer was observed which was not known initially. A further observation was that the thinnest beams (50 nm thick) were all more or less twisted after FIB-cutting from the free-standing membrane. This seems to be the reason for very different behaviours of this type of beams (green triangles in Fig. 10b). Since twisting is caused by relieve of residual stresses which also affect the IIT results, the 50 nm thick beams unfortunately had to be excluded from the study.

Fig. 11a clearly shows that the effective indentation moduli are still affected by the silicon substrate and the silica interlayer (in case of the 200 nm thick film). Only the 500 nm and 100 nm thick films allow determination of a reasonable film modulus by extrapolation to a displacement to film thickness ratio of 0. On the other hand, by taking substrate and interlayer properties into account reasonable film moduli were obtained for the 100, 200 and 500 nm thick silicon nitride films, as shown in Fig. 11b. The much lower modulus calculated for the 50 nm thick film is attributed to the impact of residual stresses, as already discussed in the previous section.

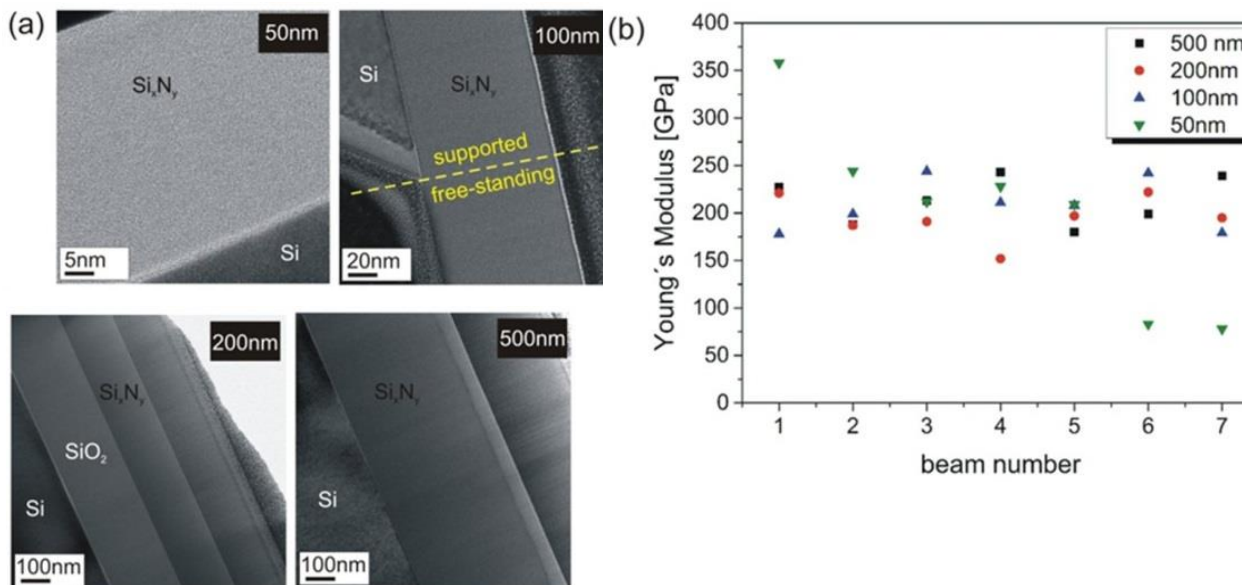


Fig. 10 (a) Cross-sectional TEM images of the amorphous silicon nitride films (not indicated layers are deposited platinum films protecting the surface during FIB machining); (b) Young’s Moduli for nominally 50 nm, 100 nm, 200 nm and 500 nm thick silicon nitride beams measured by bending.

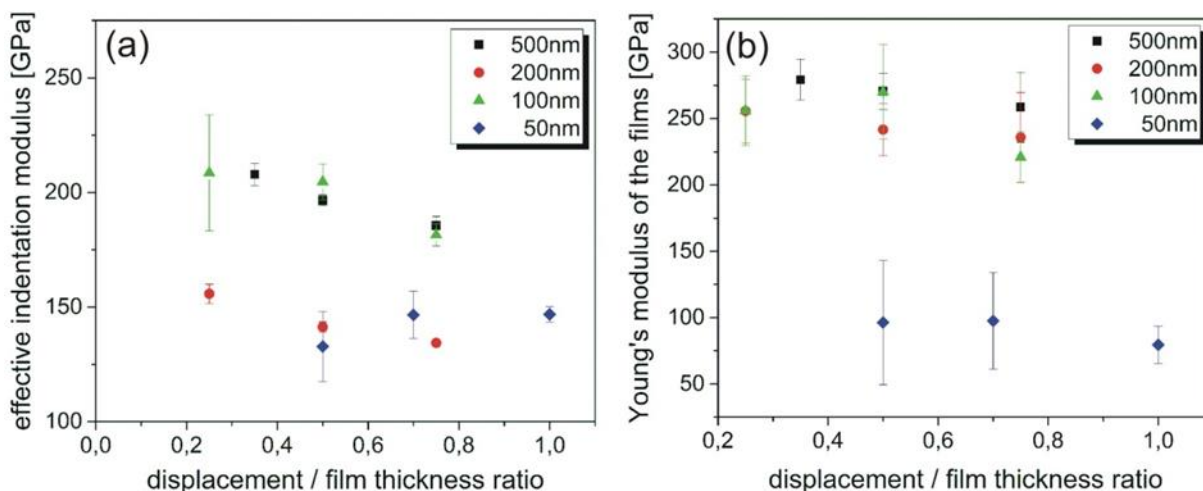


Fig. 11 (a) Effective indentation moduli for the nominally 50 nm, 100 nm, 200 nm and 500 nm thin silicon nitride films on a silicon substrate, calculated by the Oliver& Pharr-method; (b) Young’s Moduli for the nominally 50 nm, 100 nm, 200 nm and 500 nm thin silicon nitride films on a silicon substrate without influence of the substrate calculated with the software ISA. (*Error values are only given for the statistical errors.)

The mean Young’s Moduli determined with the two independent methods show a discrepancy of 50 GPa which cannot be explained by statistical errors. Since furthermore, each of the two methods suffers from a number of uncertainties which cannot be excluded unambiguously, a reliable property value cannot be attributed to the studied material. The methods based on two completely different models implying a lot of assumptions and simplifications especially when the film thickness tends to the nanoscale. Originally the determination of the Young’s Modulus was realised by tensile testing and plotting stress-strain curves, where the Young’s modulus represents the initial linear slope. To make sure that tests are comparable one has to know the exact sample geometry and the same conditions for testing have to be realised since the

Young's modulus depends on the temperature, humidity and strain rate. Going over to the nanoindentation a direct measurement of the Young's modulus is not possible. An indentation modulus is measured, which has generally speaking the same meaning as the Young's modulus, but the stiffness behaviour is just measured locally under three-axis load. This leads to a difference in terms of the value. In the end the indentation modulus can't be raised for the purpose of dimensioning. In contrast the bending test as a conventional method especially for brittle materials provides theoretically more explicit values. But also here are some difficulties. The Euler-Bernoulli equation as described in the text is actually valid only for small displacements. That means the displacement has to be much smaller than the thickness of the testing sample. This could not be realised within our testing set-up, because such small displacements can't be resolved accurately with the scanning electron microscope yet. With large displacements sliding phenomena occur. The solution of this problem probably lies in advanced theories like the micropolar theory. Additionally the models of both techniques are originally developed for testing at least for micro and macro samples. In this study the same were applied for testing at the nanoscale as well.

In conclusion neither the FMS method nor the nanoindentation can generate a "true value". Absolute values are just comparable within the same method executing exact the same experimental procedure. Excluding out the measurements with the 50 nm thick membranes because of difficulties with residual stresses, the relative trends observed with both methods are in good agreement. Thus a size effect for the Young's Modulus could not be observed in both studies, at least down to a thickness of 100 nm.

The elastic properties of amorphous silicon nitride films can vary within a wide range depending on processing parameters. The only recommendation which can be given towards preparation of a suitable thin film reference material down to the nanometer range is to perform the same procedure with silicon oxide films. At least for the thicker films, like the one with 200 nm thickness, the Young's Modulus of 70 GPa is accurately known, thus enabling a validation of the test methods.

3.6 Provision of a guideline for the measurement of the geometrical parameters, e.g. length, diameter, width and height of nanostructures and nano-objects and to establish correction factors considering tip-sample effects

Objective mainly achieved – A Good Practice Guide has been published advising on the measurement of geometrical properties of nano-objects. Experiments provide evidence for systematic deviations on the nm scale due to tip sample effects but further research is necessary to fully understand these effects.

Three different aspects influencing the measurement of geometrical parameters using AFM have been considered: substrate material, tip material and tip shape. Measurements are reported in order to provide evidence to support the conclusions presented. Unless stated otherwise, atomic force microscope (AFM) measurements were taken in a semi-clean, temperature controlled room (20 ± 0.1 °C) using an AFM with a fibre interferometer with light at 785 nm to detect the cantilever deflection and an NPL Plane Mirror Differential optical interferometer, fibre-fed with a frequency stabilised laser (632.8 nm) to traceably measure the height of the features on the surface. The noise level of the AFM was lower than 0.3 nm. For measuring the tip shape, needed for tip-sample interaction evaluation, the blind tip reconstruction technique was implemented. Further on the effect of tip wear and tip material on AFM measurements was investigated comparing a sharp and a blunt tip.

The results show an increase in height of an average of 4 nm in the case of contact mode (CM) operation and a reduction of the measured height of 1 nm for non-contact mode (NCM) operation. These effects were attributed to the different interaction between tip/sample and tip/nanoparticle depending on the tip radius. Therefore firstly we suggest that NCM is used instead of CM for measuring NP and nano-objects in general. CM could apply an excessive force to the nano-objects and cause their deformation, or even move them if not properly anchored to the substrate.

Secondly we suggest checking the level of adhesion using force distance (FD) curves. Given that FD curves can contribute to tip erosion, it is important to leave the FD curve as last test, so as to prevent altering the shape of the tip during series of measurements.

The influence of different tip materials on the measured height of nanoparticles was also investigated. A reduction of ~1 nm in the average of the measured height of the nanoparticle was observed when using a diamond tip instead of a silicon tip. Thus the used tip material itself does not influence the dimensional measurements. What was noticed, is a change in the measurement associated to tip wear. Further investigation of this effect is recommended, in particular relative to the effect of the scan parameters such as oscillation amplitude or amplitude damping for NCM AFM scans. We suggested that the variation in diameter is due to the change in contact area for both CM and NCM. For the aim of measuring the dimensions of nano-objects, we recommend that the measurements are taken with the sharpest possible tip available. This is because adhesion effects have a larger influence with blunter tips, and, therefore, minimising the contact area between tip and substrate or sample contributes to minimise these effects.

For the particles measured, we did not observe any trend associated with the substrate in the measurement of the NP's height. Finally, in this case the diameter was extracted by using the height measurement from AFM images and the effect of adhesion could be measured directly. In the case of extraction of the diameter from the lateral dimensions of the nano-objects, further sources of uncertainty need to be considered (e.g. uncertainty on the stage position, size of the scan steps, etc.). Among these is the shape of the tip. It is known that the AFM image is the dilation of the sample by the tip and therefore, whereas the height of the features mainly remains unaffected by the shape of the tip, their lateral dimensions are highly influenced. Also in this case, using a sharp tip helps reducing the uncertainty, however, for better results, "eroding" the AFM image by the shape of the tip is a further improvement. For this purpose, knowing the shape of the tip is a requirement and can be achieved by different methods such as using ad-hoc samples (e.g. "tip characterisers" or "tip check"), using SEM images of the tip or using software techniques, e.g. the "blind tip reconstruction" routine.

The work on this topic was published in a Good Practice Guide entitled "Key criteria for the determination of geometrical properties of nano-objects under different adhesion levels", which is available on the project website (<http://www.ptb.de/emrp/2618.html>).

3.7 Provision of a guideline for the preparation of fixed nano-objects on hard substrates, like nanoparticles, and nanowires

Objective achieved – A Good Practice Guide has been published advising on the fabrication of nano-objects including the fixing of nano-particles with a PMMA layer of 40 nm thickness.

Nano-object samples for reliable nanomechanical measurements in the contact mode were developed in two ways. One solution concentrated on different methods applying drops of fluids with dissolved nano-objects to cleaned samples and to dry the fluid [14]. The second approach tightly fixed nano-particles to a substrate by embedding them into a 40 nm thin PMMA layer [15].

3.7.1 Guideline for the preparation of fixed nano-objects on hard substrates using dissolved NPs

The fabrication of these nano-objects is described in a Good Practice Guide which is available on the website of the project (<http://www.ptb.de/emrp/2618.html>). It consists of the steps: substrate cleaning, calculation of the desired particle surface concentration, application of a small preparation volume of nano-object solution onto the substrate and drying.

Substrate cleaning

The substrates were selected corresponding to the requirements of the project partners. In collaboration with PTB, BAM, NPL and MIKES it was decided to investigate very flat substrates with a high degree of hardness, such as silicon wafers. For the preparation of nanowires a mica substrate was chosen.

The methods adopted in wafer cleaning technology based on wet chemical cleaning techniques generate high costs for high-purity chemicals and DI-water, problems with waste disposal and safety issues. These are the main reasons for a rapidly growing interest in dry cleaning methods. Among them plasma enhanced

cleaning is one of the most effective dry cleaning techniques in removing organic contamination on silicon wafer surfaces; also CO₂ snow, cleaning stripes and pulsed laser cleaning can be applied.

Particle surface concentration

To deposit nano-objects in a defined distance to each other it is necessary to calculate an appropriate particle surface concentration c_A [1/mm²], the particle number per substrate area:

$$c_A = \frac{N_P}{A_{PR}} = c_N \cdot \frac{V_{PR}}{A_{PR}} = c_V \cdot \frac{6}{\pi x^3} \cdot \frac{V_{PR}}{A_{PR}} = c_m \cdot \frac{1}{\rho_s} \cdot \frac{6}{\pi x^3} \cdot \frac{V_{PR}}{A_{PR}} \quad (1)$$

(surface concentration c_A , number concentration c_N , volume concentration c_V , mass concentration c_m , depending on particle size x , preparation area A_{PR} and preparation volume V_{PR} (for spherical particles))

Conventional drop drying

In case of drying, the nano-objects were deposited by liquid droplet application with following fluid evaporation if the gaseous phase still isn't saturated with vapour. The drying method was applied to all of the selected materials. The application of the conventional drying method has some drawbacks like the formation of drying rings, the crystallisation out of soluble electrolytes for particle stabilising during drying, classification effects in case of polydisperse suspensions, convection inside the droplet during evaporation and increasing stabiliser concentration in the droplet may cause particle flocculation or concentration gradients over the deposition surface. Investigations have shown drop drying in an ethanol vapour atmosphere (using Marangoni Effect) helps to overcome these problems. Opportunities to improve the particle separation are the use of an organic solvent (lower surface tension) or peptiser. Within MechProNO the suspensions were used exclusively in original to avoid artefacts that can affect the AFM measurements.

Drop-Drying by Marangoni Effect

To overcome the drying rings as well as better nano-object separation and uniform deposition over the silicon surface the Marangoni-Flow-Assisted Drop-Drying can be applied. The aqueous nano-object suspension with high surface tension pulls more strongly on the surrounding liquid with low surface tension (ethanol vapour atmosphere). The presence of a gradient in surface tension will naturally cause the liquid to flow away from regions of low surface tension. This flow induces a strong recirculation in the droplet, removing particles from the contact line and moving them along the free surface toward the droplet centre. A more uniform particle deposition results.

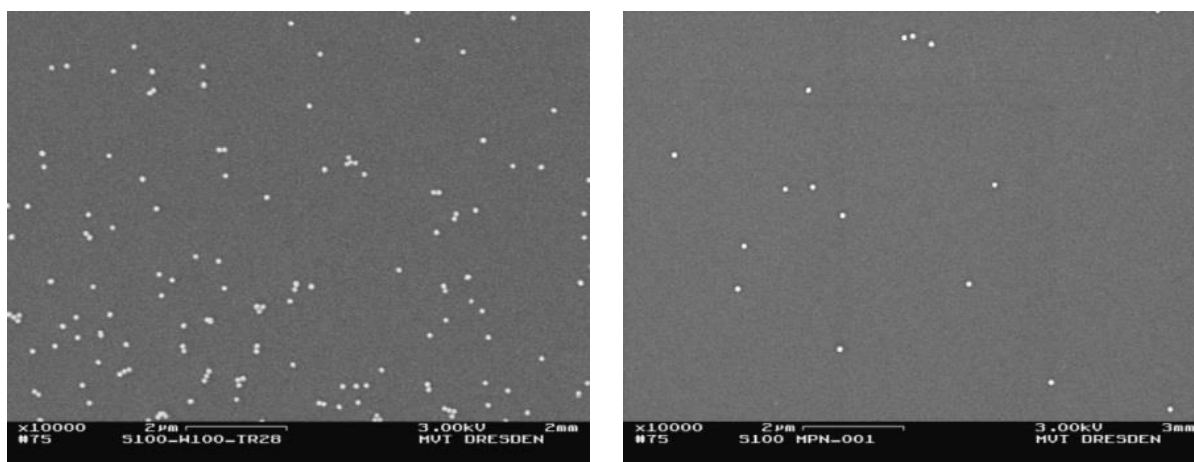


Fig. 12 Silica 100 nm particles prepared on silicon wafers by drying (left: conventional, right: electrostatic precipitation)

Rinsing

In Rinsing the nano-object deposition is realised by diffusion (based on Brownian motion) during the particle contact to the substrate. Particularly in case of titanium dioxide the rinsing method is suitable and well-reproducible.

Dip-coating

In the so-called Dip-coating method the particle deposition is effected by diffusion (based on Brownian motion) during the immersion of the substrate in a nanoparticle suspension. This preparation method was applied to all of the selected materials with the aim of producing not-clustered particles.

Electrostatic precipitation

Previous studies have shown that the electrostatic deposition of aerosols within Electrostatic Precipitators (ESP), in which the particles are deposited by electrostatic field forces, can provide substrates with separated particles depending on the quality of the generated aerosols.

To avoid re-agglomeration or sedimentation, particulate suspensions are provided in combination with stabilisers. The stabilisers are the source for residual particles during typical aerosolisation processes with atomisers. Thus, it is difficult to distinguish between target particles and residuals.

To advance this problems and to obtain very fine raw aerosols (in size range below 100 nm), to aerosolise the colloidal suspension we've also operated an Electro spray Aerosol Generator (ESG Model 3480, TSI Inc., Shoreview, USA) in combination with an ESP (Prototype of NAS Model 3089, TSI Inc., Shoreview, USA). The employed ESP consists of a corona needle as ion-source for unipolar, negative particle charging. Afterwards, the charged particles are passed through an electrical field where they are moved on the lines of electric flux to the substrate. The specific surface particle deposition rate depends on the material characteristics and the presence of stabilisers.

3.7.2 Fixing of NP by embedding into a thin layer

The fixing of nano-objects by embedding into a thin layer is described in a Good Practice Guide entitled "Good Practice Guide for nanoindentation of nanoparticles embedded in a layer using an SEM in situ technique" which is available on the website of the project (<http://www.ptb.de/emrp/2618.html>).

The particles to be tested were two sizes of silica spherical particles, nominally sized 300 nm and 100 nm in diameter, gold spherical particles, nominally sized 60 nm in diameter, and two sizes of gold rods, nominally sized 25×77 nm and 25×66 nm. They were dispersed or embedded in PMMA on a silicon substrate.

To test unbound particles, they were dispersed in solution by ultrasonification, pipetted onto the silicon substrate and left to dry.

To embed the particles on the silicon substrate using PMMA, they were dispersed in anisole and ultrasonicated for 15 minutes. After this, with the ultrasonication still running, 2 wt% PMMA was added and left a further five minutes to fully dissolve the PMMA. A drop of this was pipetted onto the silicon on a spinner, which was ramped to 500 rpm and held for 20 s. It was then ramped quickly to 5000 rpm and held for 30 s. 2 wt% PMMA in anisole under these conditions is expected to produce a film slightly under 40 nm in thickness. It was heated on a 160 °C hotplate for 60 s to drive off the solvent and harden the film. The substrate with particles now embedded was placed in 100 W oxygen plasma for 10 s, which stripped the surface of PMMA and exposed the tops while retaining them on the substrate. Imaging in the SEM revealed that the particles had agglomerated and formed spheres of different sizes, as shown in Fig. 13a

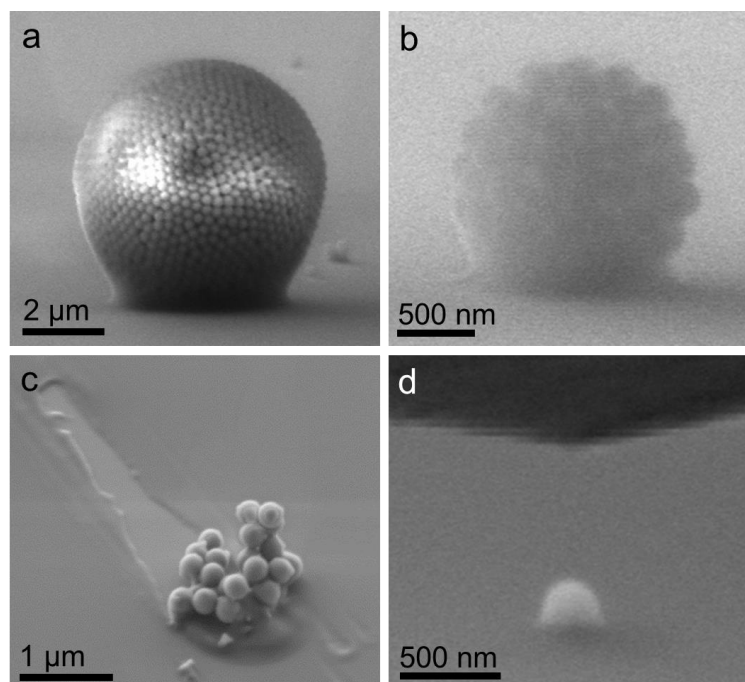


Fig. 13: 300 nm particles in PMMA a) in large spherical agglomerate, b) in a smaller spherical agglomerate, c) cluster of particles with the silicon substrate exposed. Imaging conditions: stage tilt 45°, 2 kV, WD 6 mm, d) single particle with indenter positioned above.

and b, but many single particles had also had large separations from their nearest neighbours. The remaining PMMA layer can be clearly viewed in Fig. 13c where some of the layer is missing, exposing the

substrate and revealing the thickness of the layer. A single particle is shown in Fig. 13a just behind the agglomerate, and a more isolated single particle suitable for testing is in Fig. 13d. There were also a few much larger agglomerations on the substrate that could be seen by eye. It is possible that longer ultrasonification would disperse these a bit better.

The particles were indented with and without the PMMA layer. The purpose of using PMMA was to hold the particles in position so they can be located before and after indentation, however the additional material to the particle and substrate (PMMA) complicated the results due to not fully understanding its properties. Even though the nominal thickness is known, the exact distribution of the PMMA was difficult to image due to resolution even in the SEM. However it can be seen in Fig. 13 that there is a meniscus visible at the base of the agglomerates in Fig. 13a and b, the single particle in Fig. 13d and the thickness in Fig. 13c where some of the PMMA has come away from the substrate. By indenting the particle on the substrate without the PMMA layer, a comparison of the two tests can be made to calculate the influence of the PMMA layer on the results.

A sample from each particle size were dispersed and embedded on a silicon substrate starting with the largest. The samples were indented in turn with decreasing particle size until the experiment was no longer possible.

The indenter system used to conduct the tests was an ASMEC UNAT-SEM2 in situ nanoindenter in a Carl Zeiss Auriga 60 FIB-SEM, with a Berkovich tip installed. The nanoindenter was fitted onto the stage in the microscope chamber. The stage was then tilted to 10° in order to view the indenter at the sample surface at an 80° incident angle with the electron beam. The nanoindenter required compliance calibration and load calibration for experiments at non-zero tilt.

To indent a particle, a single isolated particle was located and the indenter manually positioned approximately 1 µm above it using SEM imaging as a guide. This was done by moving the sample stage on the nanoindenter in X and Y directions. Before positioning over the particle, a test indent is made to the side to check Y positioning is correct before moving to the correct X position. Due to thermal or systematic instabilities, the indenter drifts slightly (approximately 1 nm/s) in the indentation axis. There was also some hysteresis when positioning the indenter in the Z axis.

Once the test is running, the piezo stage takes over and the indenter Z displacement is controlled more accurately. The tests were displacement controlled and the same indentation profile was used for all tests, including the substrate only tests. The total displacement was set at 1 µm, where the indenter was positioned between 0.9 µm and 1.1 µm above the substrate. It was not possible to position at the exact same height for every test, due to the hysteresis and drift associated with manually positioning the indenter. The indentation rate was 40 nm/s – 25 s to the maximum displacement of 1 µm, the maximum displacement was held for 30 s, the unload rate was 53 nm/s – 15 s to back off to 0.8 µm, this displacement was held for 30 s, and the final unload to 0 nm displacement was 5 s.

300 nm particles were measured as $\phi = (260 \pm 10)$ nm in the SEM. The particle appeared to completely flatten under maximum load, but swelled again slightly when unloaded, leaving a dimple in the middle, as shown in Fig. 15 (test B, C, and D). The load displacement curves show multiple gradients indicating the differences in the four particles reported. The indenter started highest above the substrate in test A (~1.1 µm) and was lower for each subsequent test where test D was the lowest (~0.8 µm). This accounts for different maximum loads. However, loads at different steps on the load-displacement curves differ between tests. Tests A and B show the PMMA layer and silica particle compression stages, test C shows the PMMA layer, silica particle and silicon substrate compression, and test D shows only the silica particle and silicon substrate. For test D, the PMMA layer compression stage was likely present at the start but cannot be seen because the load increased to double the other tests, obscuring the step (as also shown in the load-time curves in Fig. 16). All four tests showed the load increasing rapidly and dropping off during holding at maximum displacement. The unloading showed that plastic deformation had taken place, as the load dropped to almost zero. The SEM images after indentation confirm the plastic deformation, as they are now ellipsoids as seen in Fig. 15a-c compared to close to spherical as seen in Fig. 14. The particles were also imaged at 750 V accelerating voltage to view the surface at the best resolution in Fig. 15d-f. All images in Fig. 15 are at the same magnification as the load increased from test A to C, the particles are more flattened

with a larger top surface area. The higher loaded particles also have a less pronounced indentation groove, although this may also be affected by the indenter position on the particle which would have not been exactly central in every test.

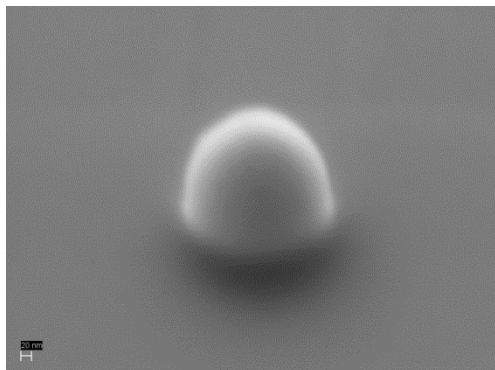


Fig. 14: Non-tested particle. Imaging conditions: sample tilt 45°, 2 kV, WD 6 mm

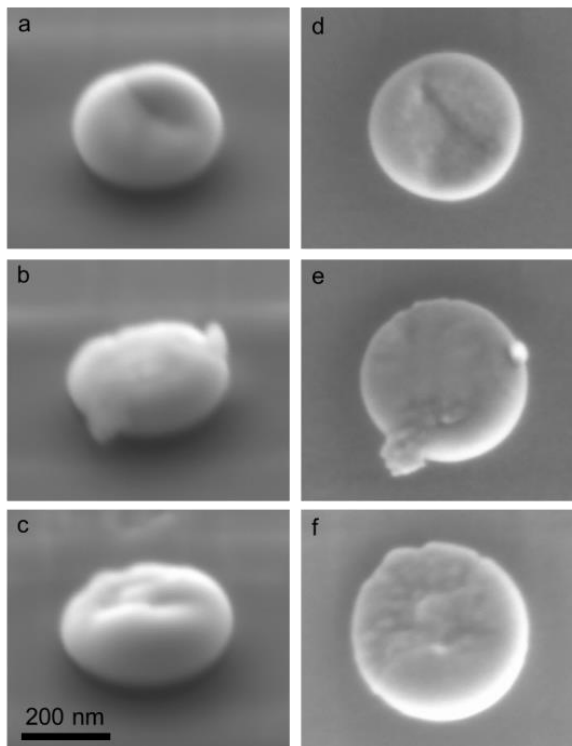


Fig. 15 (right): SEM images of indented particles a) test A, b) test B, c) test C. Imaging conditions: sample tilt 45°, 2 kV, WD 6 mm. d) test A, e) test B, f) test C. Imaging conditions: sample tilt 0°, 750 V, WD 4 mm.

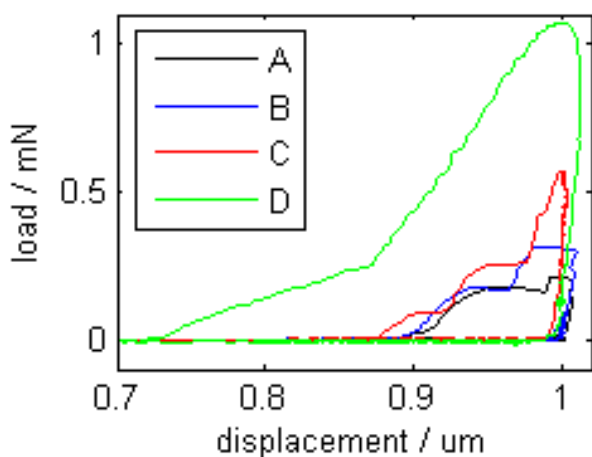


Fig. 16a: Load against displacement for indentation of four 300 nm particles in PMMA

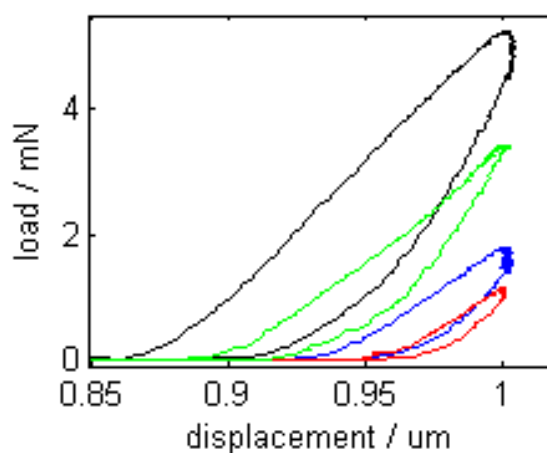


Fig. 16b: Load against displacement plots for four indents on substrate with PMMA layer

By testing the substrate, the gradient on the full tests can be compared to distinguish between indentation of the nanoparticle and of the substrate. The test conditions for indents on the substrate were the same as with previous indentation of the particles. Also similarly, the position of the indenter above the substrate could not be finely controlled, leading to different maximum loads for each test. There was some plastic deformation, as hysteresis was observed in the load-displacement graph in Fig. 15, and an indent was left behind in the substrate after testing. During the hold at maximum displacement, there was a small drop in load in some tests, but did not show the dramatic drop as with the particles in Fig. 16a.

The measured size of the particle depends on SEM conditions, where the observed difference in value compared to the original stated size (AFM), dispersed, and embedded in PMMA sizes is due to the variance in image noise depending on the technique.

It was not possible to measure the thickness of PMMA using SEM technique, as PMMA at this thickness is electron transparent. It was deduced that it is nominally 40 nm on the top of the substrate, thinner underneath the nanoparticle, and none on top of nanoparticle. The PMMA layer was also not uniform around the particle, showing build-up around the bottom. It also should be noted that the PMMA may cause apparent hardening due to prevention of expansion at the sides of the nanoparticle.

Indentation of embedded 300 nm nanoparticles is possible using a Berkovich indenter and force-displacement curves can be obtained. These showed multiple stages where the PMMA layer, nanoparticle and substrate all have different properties and therefore indented at different rates. By using an *in situ* technique in the SEM, it is possible to observe the test in real time, making it easier to locate the nanoparticles and position the indenter correctly.

3.8 Provision of a guide line for the measurement of the mechanical properties of small nanosized objects by AFM and IIT

Objective achieved – An introductory guide has been published on the measurement of the mechanical properties of nano-objects using AFM.

An guideline entitled “Introductory guide to measuring the mechanical properties of nano-objects/particles with AFM on flat surfaces” to measuring mechanical properties of nano-objects on flat substrate with AFM was published on the website of the project [16]. The original scope of the guides was adapted to the experiences gained during the project. The guide covers issues including AFM cantilever stiffness calibration, force-displacement curve measurement, cantilever bending, indentation of nanoparticles, keeping them in place and the measurement of contact area using a polycarbonate reference sample. Problems due to small, loose particles on flat substrate and how to successfully indent them with AFM, along with some remarks on the possibility of measuring elastic and plastic properties of the nano-objects in terms of the continuum-mechanical classical models are presented.

The effect of air humidity was also studied using force-distance measurements with different AFM tips on silicon substrate, in different air relative humidity levels, using the humidity controlled AFM built in the project by VTT. The measurements on the effect of the water layer formed by the ambient humidity, combined with the simulations being done by REG(UH) are potentially first studies in the world combining MDC simulation and AFM force measurement on the AFM tip-sample interaction contribution of water. VTT developed a metrological AFM with the possibility to change the humidity in the measurement chamber from 20% RH to 60% RH. Changing the humidity a 10 % reduced height of 60 nm Au nanoparticles on poly-l-lysine treated mica was measured [17].

Force-distance curves and cantilever bending

Main tool in mechanical testing is the force-distance or force-displacement (f-d) curve. Fig. 17 shows the vertical movement of a sample relative to the AFM head, and the corresponding forces for loading (red) and unloading (blue) on an approximately 20 nm - 30 nm diameter palladium nanoparticle.

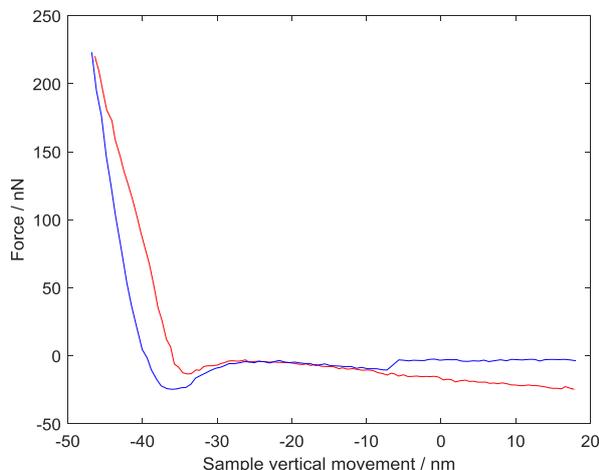


Fig. 17 Loading (red) and unloading (blue) curve indenting a Pd particle by an AFM tip. Sample movement relative to AFM head. The difference in the right side between the horizontal parts of loading and unloading curve is an anomaly in this measurement.

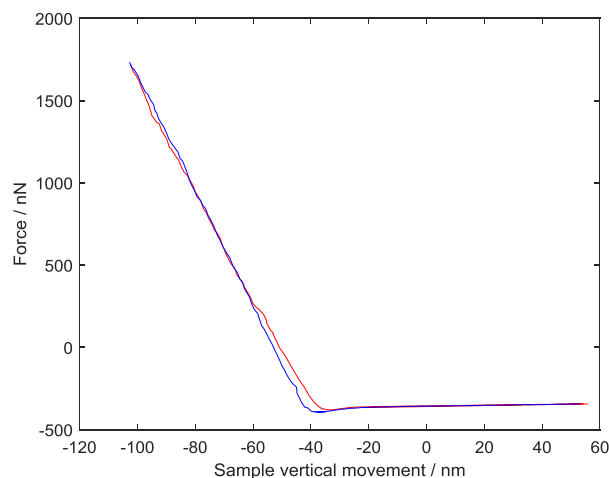


Fig. 18 Force-deflection curve for indenting the AFM tip into the silicon substrate (quite hard pushing, possibly some tip fracture). Vertical scale is in force units. Bending distance can be obtained by relating the PSPD voltage readings to the sample movement during contact to a hard sample.

Fig. 18 shows for comparison a similar curve for indenting a hard silicon substrate. Measuring the slope of the photodetector signal when pushing the tip against a hard material (or the asymptotic slope when pushing a softer material with increasing contact area), gives the conversion of photodetector signal units to bending distance of the cantilever, and thus with known cantilever stiffness, also the force scale.

However, when assessing the mechanical properties of materials, like nanoparticles, a more interesting curve is the plot of the movement of the *tip of the AFM probe relative to the sample* against applied contact force. This can be done by subtracting the cantilever bending corresponding to the PSPD values from the displacement values. When measuring very stiff or hard samples, one can also estimate and subtract the compression of the (usually silicon) AFM probe tip.

The movement of the AFM probe tip can be calculated e.g. for Fig. 17 using the slope of Fig. 18 and subtracting for each position value the cantilever bending. The result is shown in Fig. 19.

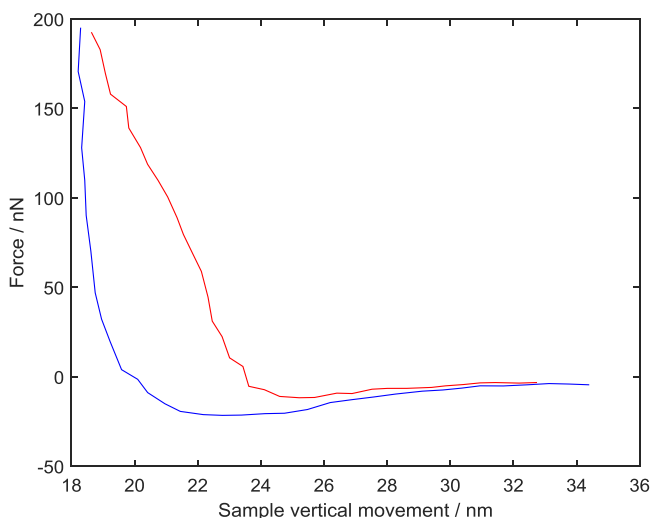


Fig. 19 AFM palladium nanoparticle indentation curve showing force versus indentation depth with arbitrary zero offset (red: loading, blue: unloading)

The calibration of photodetector values corresponding to bending in length units has to be done for each AFM probe separately because of e.g. different cantilever length and reflectance. Cantilevers with metal coated top side provide more stable and higher reflected intensity because of higher surface reflectance. In Fig. 19, it can be observed that the particle is mostly plastically deformed during loading and the unloading curve is, in this scale, almost vertical. This might also be expected since the metal particle was compressed over 10 %. In case of purely elastic deformation the loading and unloading curves overlap, excluding e.g. probe snap-in and snap-out due to adhesion forces when contacting and detaching from the particle.

Commercial AFMs can have very high resolution position sensors facilitating the calculation of curves, but due to the focus on accuracy and traceability in metrology

AFMs, metrology AFMs often have heavy sample stages and laser interferometric position measurement that may have more noise and small periodic nonlinearities that complicate the analysis of the f-d curves of nanoscale indentation experiments.

Location of the NP and keeping them in place

On flat substrates, nanoparticles that are only weakly bound to the substrate, may sometimes “escape” the AFM probe so that the probe partially slips on the surface of the particle, or the particle slips away from under the probe to another location.

The palladium particles in the examples were somewhat attached to the flat (within 1-3 nm) silicon surface due to the manufacturing process. Often it was possible to see with AFM imaging before and after f-d measurement that the particle, or part of it, was still there after testing. Also, total sudden particle escape, or tip fracture, would be seen in the f-d curve as a backward kink/jump during the loading phase. An example of particle “escaping” partly the indentation test is shown in Fig. 20.

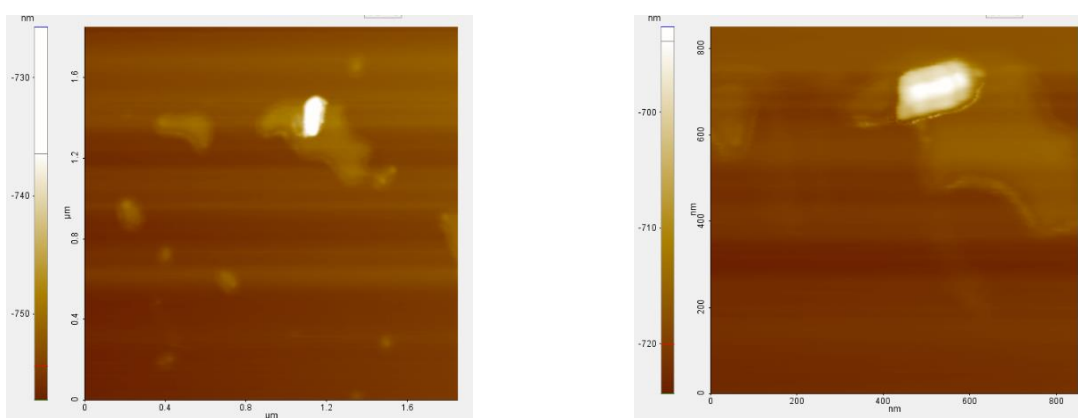


Fig. 20 A gold nanorod before (left) and after (right) f-d measurement. The images have different magnification and the shape of the AFM tip make the rod appear artificially wider in the Y direction especially in the image after indentation (right). The AFM tip has probably displaced and rotated the gold nanorod by hitting it to its side. The gold nanorod was deposited on the mica surface from applied liquid nanorod suspension. In the f-d graph the cantilever bending is not subtracted. The force rises until the nanorod starts to slip away and finally the tip meets the substrate and force starts to rise accordingly.

Attaching particles to substrates by coating the sample and then removing most of the coating has been tested in the MechProNO project (s. 3.7.2). Another method to better hold particles in place during indentation is to use not-entirely-flat substrates with grooves or pits.

Another challenge in measuring nanoparticles is their small size. A 10 nm diameter particle may easily, because of e.g. thermal drifts in the system, drift away from the apparent place where it was imaged, before the indentation with the AFM tip is done.

The indentation on the palladium particles was done with a slow laser interferometrically traceable metrology AFM so that the XY scanning of the custom-built AFM with commercial AFM controller running the Z piezo was stopped, i.e. XY scanning was paused right over the particle, and then the f-d curve measurement mode of the Z controlling system was used to make the f-d measurement. This was useful for minimising drift, scanning hysteresis and similar effects that can result if the whole AFM image is taken first and then locations selected from the image are used after imaging for f-d measurement.

One indentation can last from a few seconds to a minute depending on instrument parameters and settings and measuring one AFM image from less than a minute to several hours. If the instrument with sample has been in a thermally stable environment, powered on already for a few hours, the drift can be in the order of just 1 nm/minute, but with changing temperatures it can be several orders of magnitude higher.

Light-weight stages with small scan range can have very small stage noise, but often e.g. metrology AFMs can have several nanometres of stage noise. These factors can result in movement of the tip on the particle during indentation, or missing the particle altogether.

Contact area, f-d curve and mechanical stiffness

Estimating the apex radius/form of the AFM probe in addition to the f-d curve measurement enables one to estimate stiffness properties of the nano-object, and to compare to e.g. atomistic simulations or bulk material values in larger scale. Apex estimation can be based on e.g. electron microscopy or indentation experiments on reference materials, or ensuring the tip has a flat bottom in the scale of the objects measured.

The f-d curve in itself, possibly with information of tip size and shape, can tell about the stiffness of the object in a rather direct way. However, to get to the classical continuum mechanical properties of the particles and their material, e.g. the Oliver and Pharr model for relating contact area and probe stiffness to elastic moduli and Poisson ratios of tip and sample, or the classical models for contact like Hertz model can be applied. This has several obstacles, since the continuum models naturally do not work perfectly near the scale of single atoms - and with the tiny apex of the AFM tip, with reasonable indentation depths the slope of the upper part of the unloading curve, that can be used to analyse elastic modulus and behaviour, happens during so small a displacement that position measurement noise can prevent estimating the slope with any accuracy at all.

Nevertheless, with suitable bulk reference material, vertical position sensor, indentation depth and tip radius, and cantilever stiffness, the Oliver and Pharr model might be usable for estimating the contact area of AFM tips for use with nano-object indentation.

Measuring e.g. bending stiffness of nanowires/beams with AFM probe is a measurement that suffers less from these known complications, since contact area does not play such an important role there. It is to be noted, that in the nanoscale, the adhesion forces between tip and sample, due to e.g. Van der Waals and ambient humidity can be in the same order of magnitude as the indentation forces, possibly complicating the analysis.

3.9 Provision of uncertainty budgets related to the measurement of mechanical properties, such as elastic modulus

Objective achieved – uncertainty budgets for the measurement of the elastic modulus were obtained, proving a measurement uncertainty of less than 10% using the new device developed by the project.

BAM developed a new method for the measurement of the elastic modulus of small micro-sized beams using the bending method inside the vacuum chamber of a scanning electron microscope. The bending is realised by a micromanipulator equipped with a cantilever force sensor with an integrated tip. The nanobeams to be tested were cut out of commercially available free-standing silicon nitride membranes by the Focused Ion Beam (FIB) technique. Only few parameters have to be checked for the determination of the Young's Modulus:

- the correct force
- the displacement and
- the geometry parameters of the beams

Especially for brittle materials as silicon nitride the bending test is a suitable method in comparison to tensile testing, where no or less information about the deformation capability are available out of the measuring set-up. In a bending test this information can be extracted easily by the detection of the displacement.

A detailed uncertainty budget for the new method was set-up. FEM calculations support the required information. The work was published in a contribution intitled "Elastic property measurement of nanobeams by cantilever force measurement inside a Scanning Electron Microscope" published on the project website ([18], <http://www.ptb.de/emrp/2618.html>). The report clearly shows potentials and limitations of the used technique on a practically examined testing system. Moreover it gives recommendations how to prepare such a test on a thin solid film system and which parameters are important to obtain reliable results.

Experimental details

The beams investigated are amorphous silicon nitride beams with a thickness of 50 nm, 100 nm, 200 nm and 500 nm, a width of 2 μm and different lengths.

The beams were bent with a Force-Measurement-System (FMS) FMT-400 from Kleindiek Nanotechnik, Germany. This system is an extension tool for a micromanipulator from the mentioned supplier. The tool is equipped with a 400 μm long silicon cantilever with an integrated piezo-resistive deflection sensor. A deflection of the cantilever sensor results in an output voltage signal. The FMS is mounted in the vacuum chamber of the SEM and every step can be observed.

Before starting to measure on the silicon nitride beams, the system has to be calibrated (s. Objective 3). A second parameter has to be checked before starting to measure: the stiffness of the used FMS cantilever sensor. During the test a bending of the cantilever should not take place. This is the case for maximum forces below 7 μN . The silicon nitride beams can be tested now. Fig. 21 shows a measurement curve.

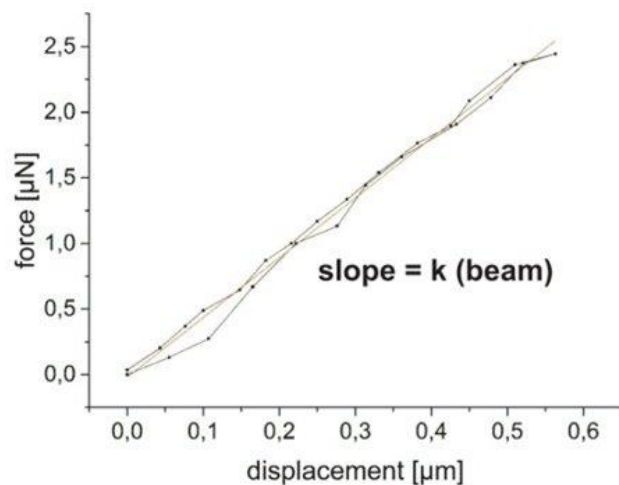


Fig. 21 Force-deflection curve of a silicon nitride beam measured by the cantilever force sensor FMS inside the SEM

Evaluation

The real thicknesses of the silicon nitride beams were determined by TEM. Seven tests were done per thickness with seven beams of similar dimensions. The detected force signal of the FMS software and the manually measured displacement were correlated for each bending test. The resulting curve was fitted linearly and a stiffness value k (the slope of the curve) for the tested object was obtained. With the exact measured geometry of the beam – in this case a rectangular one - a Young's Modulus can be calculated according to the Euler-Bernoulli equation:

$$E = \frac{4 \cdot L^3}{W \cdot T^3} k \quad (1)$$

with the effective length L , width W , thickness T and beam stiffness k . For the nominally 100 nm, 200 nm and 500 nm thick beams the values are more or less stable (s. Fig. 10). The obtained Young's Moduli are listed in Table 1.

Table 1 TEM measured thicknesses and mean Young's Moduli obtained by the FMS method

| Nominal thickness T [nm] | TEM measured thickness T [nm] | Young's Modulus mean value E [GPa] |
|----------------------------|---------------------------------|--------------------------------------|
| 50 | 50 | (202) |
| 100 | 97 | 209 |
| 200 | 182 | 195 |
| 500 | 515 | 213 |

In the literature lots of different values can be found for thin film amorphous silicon nitride: 210 GPa – 350 GPa for 100 nm to 500 nm thin beams measured by resonance spectra [19], 100 GPa – 300 GPa for 200 nm thin films deposited by various techniques measured with IIT [20], and about 250 GPa for 160 nm thick film using bulge testing [21]. The calculated values in this study fit into the range given by the literature.

Uncertainty budget

The uncertainty for the force value can be set to about 10 %. The measured displacement has to be considered with an error of about 1%. In most of the cases the tip and the surface of the tested beam were

not exactly at 90°. The positioning of the tip was roughly done by hand before the whole equipment is pumped in the SEM. The tip can't be rotated. Here the uncertainty of 1 % can be estimated additionally for the force value. All the mentioned errors influence mainly the stiffness k , which is directly proportional to the Young's Modulus. Further uncertainties are the geometry parameters of the beams, which have a much larger influence on the resulting value. First the uncertainty of the width and the length of the tested beam amount to 3 % for the error in SEM length scale measurement. The possibility that the tip slides some nanometers on the smooth beam surface during large displacements - and therefore changes the effective length of the beam - was considered in the calculation of the Young's Modulus. The thickness of the silicon nitride film was determined by TEM as exactly as possible, because this parameter is multiplied by the negative third power in the Euler-Bernoulli equation. Nevertheless an uncertainty of 3 % has to be taken into account for the TEM thickness measurement.

An error propagation calculation can be done for all the termed error sources and Table 2 shows the obtained values.

$$\Delta E = \sqrt{\left(\frac{4 \cdot L^3}{W \cdot T^3} \cdot \Delta k\right)^2 + \left(\frac{12 \cdot k \cdot L^2}{W \cdot T^3} \cdot \Delta L\right)^2 + \left(\frac{4 \cdot k \cdot L^3}{W^2 \cdot T^3} \cdot \Delta W\right)^2 + \left(\frac{12 \cdot k \cdot L^3}{W \cdot T^4} \cdot \Delta T\right)^2} \quad (4)$$

There are some more uncertainty sources which can influence the mechanical behavior and the result. The beams were machined with the help of Gallium ions. These ions are implanted in the material and thus may change the composition and mechanical properties within a superficial layer of the tested beam. In a former study we found out that this implantation depth can be set to maximum of 10 nm for 30 kV ion beam at the edges of the tested object, which is less than 1 % damaged volume of the whole object [22]. Thus the influence of the implanted ions can be neglected here as well as the presence of intrinsic stresses in the film which should be completely released by cutting free the membrane. One important evidence on intrinsic stress is the buckling of the released structure [23], which was observed only in case of the 50 nm thick film.

Usually the beam is bended at the end, but concerning the instrumentation setup it is difficult to strike the exact end position. To estimate this uncertainty, corresponding force-displacement-curves were simulated by FEM.

Table 2 Calculated uncertainty values of the Young's Modulus of amorphous silicon nitride beams measured by bending using a FMS force sensor in a SEM

| Thickness T [nm] | Young's Modulus E [GPa] | Standard deviation of E | Uncertainty ΔE | |
|-----------------------|------------------------------|------------------------------|------------------------|----|
| | nominal mean value | [GPa] | [GPa] | % |
| 100 | 209 | 24 | 21 | 10 |
| 200 | 195 | 22 | 15 | 8 |
| 500 | 213 | 25 | 20 | 9 |

Finally to complete the list of uncertainties both the elastic-plastic deformation of the FMS tip and the thermal drift has to be taken into account. These errors should be very small, because the tested objects are quite soft compared to the tip and the FIB/SEM room was under climate control.

Summary

- PTB set-up a new measurement capability of calibrating cantilever normal stiffness ranging from 0.01 N/m to 1000 N/m with an uncertainty of 5 % based on new MEMS reference springs

- PTB developed new reference springs for the simultaneous calibration of force and displacement of atomic force microscopes and nanoindenters in the micro Newton range up to 12 μN and up to 3 μm displacement.
- BAM and PTB developed a new nanoindentation reference method for the measurement of Young's modulus of high aspect ratio micro- and nanopillars. It revealed that the equivalent stiffness of the pillars has to be taken into account for reliable elastic modulus measurements [10]. Comparable indentation moduli compared to the bulk material resulted and no size effect was observed.
- VTT developed a new measurement capability for nanomechanical AFM measurements under different humidity levels in order to investigate its influence on the measurements. In a cooperation with the University of Helsinki indentations of gold nanoparticles were simulated using molecular dynamic calculations and compared with measurements.
- A new measurement capability for in-situ bending tests was established at BAM. Reasonable elastic modulus results with uncertainties of 10 % were obtained for silicon nanowires and sub-micron beams cut from membranes. The method is not new, but its combination with IIT at the same material, partly supported by a substrate and partly as free-standing membrane is new in the world.
- New measurement capabilities for the dimensions of nanoparticles are available at NPL including the measurement of AFM tip shape via blind tip reconstruction.
- NPL developed a new measurement capability for the nanoindentation of nanoparticles in a SEM supported by FEM.
- Two techniques for fixing nanoparticles to substrates were developed. TU Dresden developed methods using nanoparticles in solutions and NPL invested methods to embed nanoparticles in a PMMA matrix.

4 Actual and potential impact

The impact of the project is directly related to the provision of methodologies, calibration and test tools, and improved analytical tools for modelling and simulation of indentation measurements with AFM. Best practice guides for improved measurement of size, shape and mechanical properties of nanoscale objects were developed and made available to interested scientists via the project web page [1]. Project results were also publicised by a tutorial offered to the public at the TU Dresden. The presentations are available online (<http://www.ptb.de/emrp/782.html>).

Further dissemination activities included offering micro- and nano-object samples developed during the project to interested scientists.

The following samples are available:

- Pillars (Si, 80 nm < height < 530 nm, 324 nm < diameter < 2323 nm)
- Beams (Si, SiO₂, 74 nm < thickness < 2000 nm, 0.01 N/m < nominal stiffnesses < 5 N/m)
- Bridges (Si, SiO₂, 74 nm < thickness < 2000 nm, 0.01 N/m < nominal stiffnesses < 5 N/m)
- Particles on substrates
 - Gold nanospheres (60 nm diameter)
 - gold nanorods (ϕ 25 nm x 77 nm)
 - silica nanospheres (24/100/284 nm diameter)
 - silver nanospheres (50 nm diameter)
 - titanium dioxide spheres (28 nm)

Early impact

Micro- and nanoforce metrology with AFM and IIT is now possible with lower uncertainty. With AFM it is possible to buy cantilevers whose stiffness is calibrated with an uncertainty of only 10 %. Newly developed meander or MEMS reference springs allow AFM and IIT to reduce the uncertainty further. Thus measurement techniques for the mechanical properties of nanomaterials are now more accurate and traceable. Several companies and NMIs are able to provide reference samples and services, which are essential for all measurements of nano-objects:

- AFM cantilevers are now commercially available from a stakeholder with a stiffness uncertainty of only 10 % [1]. PTB improved together with the stakeholder the most often used cantilever stiffness calibration technique, the thermal vibration method. The uncertainty of the improved thermal vibration method could be reduced by approximately 40 % to now only 10 % [7]. In future, customers can buy calibrated cantilevers and be sure that the stiffness uncertainty is not bigger than 10 %. One prerequisite for precise mechanical measurements with the AFM is realised and will help to further widen the range of AFM force spectroscopy applications.
- BAM offer a new service for the calibration of elastic modulus via Focussed Ion Beam (FIB) in-situ bending measurements of nano-beams using a micromanipulator equipped with a piezo-resistive force sensor [2]. A good practice guide describing the method is publicly available [18]. A comparison of elastic modulus measured using nanoindentation and PTB's MEMS device confirmed the performance of the new service.
- BAM are applying the new service to measure the elastic modulus of silicon nanowires [2] for the KoC University in Istanbul. The nanowires had widths of 35 nm and 74 nm and a height of 168 nm. The deviations between experiment and FEM simulation were very small. Deviations observed in the bending experiments between successive tests could be explained by uncertainties of tip positioning and specifically in the case of the smaller nanowire, by twisting of the nanowire. A further slight systematic deviation observed for the smallest wire was attributed to the influence of the very thin native oxide layer on the nanowires. In conclusion no size effect of the elastic behavior of silicon was found in this study [2].
- A new calibration service for cantilever stiffness based on calibrated MEMS [6] is offered by PTB. The new calibration device is based on calibrated MEMS reference spring actuators [4] which are fabricated by the Technical University (TU) of Chemnitz. Cantilevers with stiffnesses ranging from 0.01 N/m to 1000 N/m can be calibrated with an uncertainty of 5 %. A good practice guide describing the method is publicly available [24]. To test the new calibration setup a comparison measurement of the stiffness of one cantilever (PPP-CONTR, stiffness 0.12 N/m) with PTB's nanonewton force facility, which offers an uncertainty of only 0.6 % [25] has been carried out. The deviation of the stiffness value measured by the MEMS was less than 1 % confirming the good performance of the new stiffness calibration service.
- New meander type reference springs for the in-situ force calibration of AFMs and nanoindenters are now commercially available. The meander springs offer a very big loading area (1 mm x 0.7 mm) for force application. The springs allow the reduction of AFM force uncertainty down to 2 % [9].

Potential impact

Traceable calibrated AFM cantilevers and reduced uncertainty in stiffness will, in the long term, lead to further investigations of mechanical properties of nano-objects using AFM and help to build confidence in AFM mechanical property measurements and performance. Reliable data, combined with modelling, will allow nanomaterials to be exploited in new applications and to replace existing components. Nanomaterials have the potential to be used in the development of new materials with better mechanical properties and new functionalities, this will be facilitated by easier and more accurate mechanical property measurements. The techniques developed during the project are already being used in universities and some companies. Specifically:

- the developed new MEMS double spring for AFMs and nanoindenters will offer the possibility to separately calibrate force and deflection of AFMs and nanoindenters. The new MEMS spring consists of two springs in series with a gap of 3 μm [6]. The big advantage of these new MEMS reference springs is that they show no dependence of stiffness on the loading position on the MEMS loading area (50 μm x 50 μm) and moreover the temperature dependence of stiffness, force and deflection is below 1 % for

ambient conditions. TU-Ch is aiming at offering these MEMS double springs to customers in the near future.

- TU-Ch developed new approaches for encapsulation of the sensitive MEMS devices both on wafer as well as on chip level. The developed technology provides an open platform for further MEMS fabrication and delivery to interested partners, whereas the stiffness parameters can be easily adapted to customer requirements within a wide parameter range.

Summary of the dissemination activities undertaken

The key data of the project are the following:

- 22 publications in the public domain as listed below, and another 5 publications anticipated. Key papers included the “Determination of the Elastic Behaviour of Silicon Nanowires within a Scanning Electron Microscope” by Nicole Wollschläger published in the Journal of Nanomaterials, “In-situ non-destructive characterisation of the normal spring constant of AFM cantilevers” by Sai Gao published in journal Measurement Science and Technology (MST), “Determination of the mechanical properties of nanopillars using the nanoindentation technique” by Zhi Li published in Nanotechnology and Precision Engineering, “Nanoindentation of gold nanorods with an Atomic Force Microscope” by Bernhard Reischl published in Materials Research, “Atomistic simulation of AFM indentation of gold nanorods on a silicon substrate” by Bernhard Reischl published in the Journal of Phys. Chem. C, “Silicon double spring for the simultaneous calibration of probing forces and deflections in the micro range” by Uwe Brand published in the journal Measurement Science and Technology, “Comparing AFM cantilever stiffness measured using the thermal vibration and the improved thermal vibration method with that of a SI traceable method based on MEMS” by Uwe Brand published in the journal MST, “A deep etching mechanism for trench-bridging of silicon nanowires” by Zuhail Tasdemir published in Nanotechnology and Precision Engineering, “SI traceable determination of the spring constant of a soft cantilever using a nanonewton force facility based on electrostatic methods” by Vladimir Nesterov published in Metrologia and “Atomic force microscope adhesion measurements and atomistic molecular dynamics simulations at different humidities” by Jeremias Seppä published in Measurement Science and Technology.
- 22 presentations and posters presented at key International conferences including SPIE microtechnologies, Nanoscale Seminar on Quantitative Microscopy and Calibration Standards and Methods, Euspen conference of the European Society for Precision Engineering and Nanotechnology, Spring Meeting of the European Materials Research Society, Micro- and Nanointegration workshop of the VDE GMM, International Conference on Atomically Controlled Surfaces, Interfaces and Nanostructures ACSIN & ICSPM, Nanomeasure scientific symposium, PARTEC - International Congress on Particle Technology, Nanosafe International Conference on Safe production and use of nanomaterials.
- 5 training sessions on topics like “Preparation of nano-particles on substrates”, “Focused Ion Beam Machining for Site-specific Nanocharacterisation”, “Traceable measurement of mechanical properties of nano-objects” and “Application of Oliver-Pharr method to AFM force-distance measurements”.

5 Website address and contact details

A website is available, where the public can be informed about project news, meetings and events: <http://www.ptb.de/emrp/mechprono.html>

The contact person for questions about the project is Uwe Brand, PTB, uwe.brand@ptb.de.

6 List of publications

- [1] NANOSENSORSTM, „Special Developments List – Quick Overview of Possible Customised Solutions“. [Online]. <http://www.nanosensors.com/pdf/SpecialDevelopmentsList.pdf>. [Access: 25-Juni-2015].

- [2] N. Wollschläger, Z. Tasdemir, I. Häusler, Y. Leblebici, W. Österle, und B. E. Alaca, „Determination of the Elastic Behavior of Silicon Nanowires within a Scanning Electron Microscope“, *J. Nanomater.*, 2016, 1–6, 2016.
- [3] S. Gao, U. Brand, S. Hahn, und K. Hiller, „An active reference spring array for in-situ calibration of the normal spring constant of AFM cantilevers“, in *SPIE 9517 Smart sensors, Actuators and MEMS VII; and Cyber Physical Systems*, 2015, 951719.
- [4] S. Gao und U. Brand, „In-situ nondestructive characterisation of the normal spring constant of AFM cantilevers“, *Meas. Sci. Technol.*, 25, 4, 44014, Apr. 2014.
- [5] U. Brand u. a., „Smart sensors and calibration standards for high precision metrology“, 2015, Proc. SPIE 9517, 95170V–95170V–10.
- [6] U. Brand, Z. Li, S. Gao, S. Hahn, und K. Hiller, „Silicon double spring for the simultaneous calibration of probing forces and deflections in the micro range“, *Meas. Sci. Technol.*, 27, 1, 15601, Jan. 2016.
- [7] U. Brand, „Comparing AFM cantilever stiffness measured using the thermal vibration and the improved thermal vibration methods with that of an SI traceable method based on MEMS“, *Meas. Sci. Technol.*, 28, 3, 034010, 2016.
- [8] S. Gao u. a., „A comb-drive scanning-head array for fast scanning-probe microscope measurements“, Proc. SPIE 8066, Smart Sensors, Actuators, and MEMS V, 2011, p. 806626.
- [9] U. Brand u. a., „Round robin for testing instrumented indenters with silicon reference springs“, *Int. J. Mater. Res.*, 106, 12, 1215–1223, Dec. 2015.
- [10] Z. Li, S. Gao, F. Pohlenz, U. Brand, L. Koenders, und E. Peiner, „Determination of the mechanical properties of nano-pillars using the nanoindentation technique“, *Nanotechnol. Precis. Eng.*, 3, 182–188, 2014.
- [11] B. Reischl, A. Kuronen, und K. Nordlund, „Nanoindentation of gold nanorods with an atomic force microscope“, *Mater. Res. Express*, 1, 4, 45042, 2014.
- [12] P. Klapetek und D. Nečas, „Independent analysis of mechanical data from atomic force microscopy“, *Meas. Sci. Technol.*, 25, 4, 44009, Apr. 2014.
- [13] Z. Tasdemir, N. Wollschläger, W. Österle, Y. Leblebici, und B. E. Alaca, „A deep etching mechanism for trench-bridging silicon nanowires“, *Nanotechnology*, 27, 9, 95303, 2016.
- [14] P. Fiala und M. Stintz, „Guideline for the preparation of fixed nano-objects on hard substrates, like nanoparticles and nanowires“, *Good Practice Guides*, 2015. [Online]. <http://www.ptb.de/emrp/2618.html>. [access: 22-Sep-2016].
- [15] „Good Practice Guide for nanoindentation of nanoparticles embedded in a layer using an SEM in situ technique“, *Good Practice Guides*. [Online]. <http://www.ptb.de/emrp/2618.html>. [access: 22-Sep-2016].
- [16] „Introductory guide to measuring the mechanical properties of nano-objects/particles with AFM on flat surfaces“, *Good Practice Guides*. [Online]. <http://www.ptb.de/emrp/2618.html>. [access: 22-Sep-2016].
- [17] J. Seppä, „Atomic force microscope adhesion measurements and atomistic molecular dynamics simulations at different humidities“, *Meas. Sci. Technol.*, vol. 28, no. 3, p. 034004, Mar. 2017.
- [18] W. Österle, „Good Practice Guide “Elastic property measurement of nanobeams by cantilever force measurement inside a Scanning Electron Microscope”“, *Good Practice Guides*, 2015. [Online]. <http://www.ptb.de/emrp/2618.html>. [access: 22-Sep-2016].
- [19] K. B. Gavan, H. J. R. Westra, E. W. J. M. Van der Drift, W. J. Venstra, und H. S. J. Van der Zant, „Impact of fabrication technology on flexural resonances of silicon nitride cantilevers“, *Microelectron. Eng.*, 86, 4–6, 1216–1218, Apr. 2009.
- [20] P. Morin, G. Raymond, D. Benoit, P. Maury, und R. Beneyton, „A comparison of the mechanical stability of silicon nitride films deposited with various techniques“, *Appl. Surf. Sci.*, 260, 69–72, 2012.
- [21] Y. Hwangbo, J.-M. Park, W. L. Brown, J.-H. Goo, H.-J. Lee, und S. Hyun, „Effect of deposition conditions on thermo-mechanical properties of free standing silicon-rich silicon nitride thin film“, *Microelectron. Eng.*, 95, 34–41, 2012.
- [22] N. Wollschläger, W. Österle, I. Häusler, und M. Stewart, „Ga+ implantation in a PZT film during focused ion beam micro-machining“, *Phys. Status Solidi C*, 12, 3, 314–317, März 2015.
- [23] G. Pennelli, M. Totaro, und A. Nannini, „Correlation between surface stress and apparent young’s modulus of top-down silicon nanowires“, *ACS Nano*, 6, 12, 10727–10734, 2012.
- [24] U. Brand, „Good Practice Guide for the measurement of the cantilever normal spring constant using a MEMS device“, *Good Practice Guides*, 2015. [Online]. <http://www.ptb.de/emrp/2618.html>. [access: 22-Sep-2016].
- [25] V. Nesterov u. a., „SI-traceable determination of the spring constant of a soft cantilever using the nanonewton force facility based on electrostatic methods“, *Metrologia*, 53, 4, 1031–1044, Aug. 2016.

- [26] N. Wollschläger, P. Reinstädt, W. Österle, and M. Griepentrog, 'Comparison of two methods for the Young's Modulus determination of thin silicon nitride films: Cantilever bending and instrumented indentation technique in the micro and nano range', Internal report of the EMRP project MechProNO, 2016. [Online]. Available: https://www.ptb.de/emrp/fileadmin/documents/tmompon/documents/Publications/2015/2016_Wollschlaeger_Comparison_of_two_methods_for_the_Young_231015.pdf.